

Tectonic Trends of the Northern Part of the Paradox Basin,  
Southeastern Utah and Southwestern Colorado,  
As Derived From Landsat Multispectral Scanner Imaging  
and Geophysical and Geologic Mapping

Uncontrolled X-Band Radar Mosaic of the  
Western Part of the Moab 1°×2° Quadrangle,  
Southeastern Utah and Southwestern Colorado

U.S. GEOLOGICAL SURVEY BULLETIN 2000-C, D





**Tectonic Trends of the Northern Part of the Paradox Basin,  
Southeastern Utah and Southwestern Colorado,  
As Derived From Landsat Multispectral Scanner Imaging  
and Geophysical and Geologic Mapping**

*By Jules D. Friedman, James E. Case, and Shirley L. Simpson*

**Uncontrolled X-Band Radar Mosaic of the  
Western Part of the Moab 1°×2° Quadrangle,  
Southeastern Utah and Southwestern Colorado**

*By Jules D. Friedman and Joan S. Heller*

**EVOLUTION OF SEDIMENTARY BASINS—PARADOX BASIN**

A.C. Huffman, Jr., Project Coordinator

---

**U.S. GEOLOGICAL SURVEY BULLETIN 2000—C, D**

*A multidisciplinary approach to research studies of  
sedimentary rocks and their constituents and  
the evolution of sedimentary basins, both ancient and modern*

*Chapters C and D are issued as a single volume and are not available separately*



**U.S. DEPARTMENT OF THE INTERIOR**

**BRUCE BABBITT, Secretary**

**U.S. GEOLOGICAL SURVEY**

**Robert M. Hirsch, Acting Director**

Published in the Central Region, Denver, Colorado  
Manuscript approved for publication August 5, 1992  
Edited by Judith Stoesser  
Graphic design by Patricia L. Wilber  
Cartography by Joseph A. Romero  
Type composed by Shelly Fields  
Cover prepared by Art Isom

For Sale by U.S. Geological Survey, Map Distribution  
Box 25286, MS 306, Federal Center  
Denver, CO 80225

Any use of trade, product, or firm names in this publication is for descriptive purposes only and does not imply endorsement by the U.S. Government

**Library of Congress Cataloging-in-Publication Data**

Friedman, Jules D. 1928-

[Tectonic trends of the northern part of the Paradox Basin, southeastern Utah and southwestern Colorado, as derived from Landsat multispectral scanner imaging and geophysical and geologic mapping]

Tectonic trends of the northern part of the Paradox Basin, southeastern Utah and southwestern Colorado, as derived from Landsat multispectral scanner imaging and geophysical and geologic mapping / by Jules D. Friedman, James E. Case, and Shirley L. Simpson; Uncontrolled X-band radar mosaic of the western part of the Moab 1°x2° quadrangle, southeastern Utah and southwestern Colorado / by Jules D. Friedman and Joan S. Heller.

p. cm. — (Evolution of sedimentary basins—Paradox Basin ; ch. C-D) (U.S. Geological Survey bulletin ; 2000 C-D)

Includes bibliographical references.

Supt. of Docs. no.: I19.3:2000 C-D

1. Geology—Paradox Basin Region. 2. Geology, Structural—Utah. 3. Geology, Structural—Colorado. 4. Astronautics in geology. 5. Radar in earth sciences. 6. Paradox Basin. I. Case, James E., 1933- . II. Simpson, Shirley L. III. Friedman, Jules D. Uncontrolled X-band radar mosaic of the western part of the Moab 1°x2° quadrangle, southeastern Utah and southwestern Colorado. 1993. IV. Title: Uncontrolled X-band radar mosaic of the western part of the Moab 1°x2° quadrangle, southeastern Utah and southwestern Colorado. V. Series.

VI. Series: U.S. Geological Survey bulletin ; 2000 C-D.

QE75.B9 no. 2000 C-D

[QE627.5.U8]

557.3 s—dc20

[551.87'09792]

92-29800  
CIP

# CONTENTS

- C. **Tectonic Trends of the Northern Part of the Paradox Basin, Southeastern Utah and Southwestern Colorado, As Derived from Landsat Multispectral Scanner Imaging and Geophysical and Geologic Mapping**  
*By Jules D. Friedman, James E. Case, and Shirley L. Simpson*
- D. **Uncontrolled X-Band Radar Mosaic of the Western Part of the Moab 1°×2° Quadrangle, Southeastern Utah and Southwestern Colorado**  
*By Jules D. Friedman and Joan S. Heller*



# Tectonic Trends of the Northern Part of the Paradox Basin, Southeastern Utah and Southwestern Colorado, As Derived From Landsat Multispectral Scanner Imaging and Geophysical and Geologic Mapping

By Jules D. Friedman, James E. Case, *and* Shirley L. Simpson

EVOLUTION OF SEDIMENTARY BASINS—PARADOX BASIN

A.C. Huffman, Jr., Project Coordinator

---

U.S. GEOLOGICAL SURVEY BULLETIN 2000-C

*A multidisciplinary approach to research studies of  
sedimentary rocks and their constituents and  
the evolution of sedimentary basins, both ancient and modern*



UNITED STATES GOVERNMENT PRINTING OFFICE, WASHINGTON : 1994



# CONTENTS

Abstract.....	C1
Introduction.....	2
Geologic Setting of the Paradox Basin.....	2
Sources of Data.....	5
Definitions and Categories of Lineaments and Alignments.....	5
Mapped from Landsat Multispectral Scanner Images.....	5
Geophysical Lineaments.....	7
Analysis of Data.....	7
Evidence for Precambrian Basement Involvement in Northeast- and Northwest-Trending Structures in the Paradox Basin.....	9
Review of Geologic and Geophysical Evidence for Northwest-Trending Structures.....	9
Geologic Field Mapping and Remote-Sensing Evidence for Northwest Tectonic Trends.....	11
Review of Geologic and Geophysical Evidence for Northeast-Trending Structures.....	14
Geologic Field Mapping and Remote Sensing Evidence for Northeast Tectonic Trends.....	15
Possible Involvement of the Precambrian Basement.....	16
Time of Movement and Tectonic Significance of Northeast-Striking Faults.....	22
Summary.....	26
References.....	28

## FIGURES

1-5. Maps showing:	
1. Structural features in area of Paradox Basin.....	C3
2. Tectonic features, northern Paradox Basin.....	6
3. Magnetic lineaments, northern Paradox Basin.....	8
4. Gravity lineaments, northern Paradox Basin.....	9
5. First-order fracture patterns in area of Colorado Plateau.....	10
6. Diagram showing fracture orientations in area of Colorado Plateau.....	11
7-10. Rose diagrams showing frequency distribution of azimuthal trends, northern Paradox Basin:	
7. As mapped from Landsat multispectral scanner images.....	11
8. As mapped from Landsat multispectral scanner images, by tectonic region.....	12
9. As derived from gravity-field and aeromagnetic maps.....	12
10. Of joint sets and geologically mapped faults and folds.....	13
11, 12. Maps showing:	
11. Inferred configuration of Precambrian surface in vicinity of La Sal Mountains.....	15
12. Location of mapped and inferred faults in northern part of Paradox Basin.....	17
13. Photograph showing vertical fractures in Roberts rift fault zone.....	18
14. Structure sections of fault in Mt. Peale 2° NW quadrangle, Utah.....	19
15-17. Photographs showings:	
15. Oblique aerial view across Salt Valley anticline.....	21
16. Northeast-trending joint set in Entrada Sandstone on southwest flank of Salt Valley anticline.....	22
17. Fully developed fin topography in top unit of Entrada Sandstone.....	23
18. Diagram showing stratigraphic ages of formations cut by northeast-striking faults, northern Paradox Basin.....	26
19. Photograph showing oblique aerial view of Upheaval Dome and surrounding circular structure near Canyonlands.....	27

TABLE

1. Forty-eight northeast-trending faults giving formations cut by faults and earliest age of most recent fault movement, northern part of Paradox Basin, southeastern Utah and southwestern Colorado..... C24

# Tectonic Trends of the Northern Part of the Paradox Basin, Southeastern Utah and Southwestern Colorado, As Derived from Landsat Multispectral Scanner Imaging and Geophysical and Geologic Mapping

By Jules D. Friedman, James E. Case, and Shirley L. Simpson

## ABSTRACT

Rose diagrams prepared from azimuthal histogram plots of several thousand lineaments of the Moab 1°×2° quadrangle in southeastern Utah and southwestern Colorado permit detailed statistical comparison of Landsat multispectral scanner lineament trends with magnetic and gravity-field trends and fault and fold-axis strike trends.

A good correlation exists between trends of major Landsat lineaments (especially those longer than 20 km (12.4 mi)), magnetic and gravity fields, and northwest-trending joints, fold axes, and faults on geologic maps. A similarly good correlation exists between the first-order surface azimuthal trends of all and length-weighted lineaments mapped from Landsat imagery and inferred northeast-trending structural discontinuities of the Precambrian basement mapped from the magnetic and gravity fields. These inferred northeast-trending discontinuities of the basement complex follow a strike projection of the pre-Sinyala fault system of northern Arizona and are interpreted here as representing basement-controlled structures opened by reactivation of Precambrian faults.

Many of the northeast-striking faults and other fractures are of extensional character. Some of these structures possibly resulted from vertical tectonic activity during evolution of elongate salt diapirs within the anticlinal cores. Many of the northeast-striking faults are of Laramide to Pleistocene age on the basis of crosscutting stratigraphic relations, but many of the northeast-trending structures are basement controlled and were opened by reactivation of Precambrian faults.

The good correspondence between the first-order trends of magnetic-field lineaments (at N. 40°–60° W.), presumably representing discontinuities of the Precambrian basement, and surface lineaments and mapped joints and faults suggests that the Precambrian crystalline basement has

been involved in pre-Laramide, Laramide, and post-Laramide tectonic episodes. The northwest tectonic trends, along which salt anticlines of the Paradox Basin are aligned, suggest that the crystalline basement, already block faulted in the late Paleozoic, may have been further deformed during Laramide compression. It is possible that northwest-trending, parallel antiforms and synforms were then formed in the Precambrian crystalline rocks, the synforms providing the locus for enhanced thickening of the deep-seated keels of the salt anticlinal cores.

The trend of N. 10°–20° E. lineaments coincides with the trend of post-Laramide joint sets that have been opened to produce extensional and transtensional fractures consonant with the post-Laramide stress field.

That the laccolith complex and domal uplift of the La Sal Mountains and several other laccolith complexes were emplaced at intersections of some of the major northwest and northeast lineaments of the Paradox Basin is of special tectonic significance. The occurrence of laccolith complexes, such as the La Sal, Henry, and Abajo Mountains and others, suggests that they may have been emplaced at nodes of a northwest-northeast lineament grid. Faulting down to the depth of the crust is suggested and testifies to the deep-seated nature of the N. 40°–60° W. and N. 40°–50° E. discontinuities. Recent studies indicate a mantle source for the laccolith magmas.

Circular features such as the Lockhart Basin, beneath which salt dissolution and subsidence of the overlying Phanerozoic sequence of clastic rocks have occurred, may represent the negative analog of salt diapirism in the Paradox Basin; the generation of circular diapiric, intrusive, and subsidence structures may indeed have followed the network of rectilinear deep-seated faults. The semiconcentric Needles fault zone, localized along a northeast-trending and structurally controlled segment of the Colorado River Gorge, has probably developed in response to downcutting, subsequent unloading phenomena, and structural extension through

Holocene time as a result of gravity sliding of the Phanerozoic sequence along the surface of the salt-bearing Paradox Formation, which has been lubricated by groundwater.

Surface faults, such as fault clusters of en echelon character that lie astride the northeast-trending Precambrian structural discontinuities, and concentric or circular features, such as the Lockhart Basin and Needles fault zone, may be significant in localizing salt flowage and dissolution.

Drainage pattern analysis suggests that the northwesterly and northeasterly structural patterns and lineaments extend from the Uncompahgre Plateau at least as far southwest as Indian Creek and Harts Draw, Lavender Canyon, Davis Canyon, North Cottonwood Creek, and the Needles fault zone.

## INTRODUCTION

The objective of the Paradox Basin remote-sensing project of the U.S. Geological Survey is to interpret geologically a variety of satellite (in this chapter notably multispectral scanner images of the Landsat system) and aircraft images of the region in order to assess factors in the structural and geomorphic environment that may provide some insight into the evolution of the Paradox sedimentary basin (fig. 1).

In this region, basement structure appears to be effectively masked by a thick layer of evaporites and clastic rocks, and many geologists have assumed that surface features may not in any way resemble the structural style of deformation of strata below the geologic mask. The plan of the present study is to carry out subsurface geophysical and surface remote-sensing investigations and to map fractures, including joints and faults at the surface, with special attention to azimuthal frequency of trends and structural interpretation, without prejudging the questions of geologic masking, propagation of structures, or reflection of tectonic style through the intervening sequence of sedimentary rocks. Thus, we undertook an investigation designed to evaluate enigmatic or previously undiscerned and unmapped structural features that may have influenced, or that may reflect, the tectonic evolution of the sedimentary basin.

It is understood that parallelism of tectonic trends of the Precambrian basement complex and more recent rocks of the sedimentary sequence does not imply synonymy of structural style and processes over long periods of time, nor does it necessarily imply reactivation of older structures. But if a significant link can be established between basement structural orientation and younger features, it hardly seems wholly fortuitous.

In this paper, we present previously unpublished interpretations of trends of faults, joints, and other structures in the northern part of the Paradox Basin of Utah and Colorado and lineament trends obtained using remote-sensing and

potential-field geophysical techniques, and we review the tectonic significance of the dominant lineament trends.

*Acknowledgments.*—The authors acknowledge the considerable knowledge and insight gained from field and office discussions with Robert Hite, Eugene Shoemaker, Dennis O'Leary, Irving Witkind, and other geologists who work in the Paradox Basin and the constructive manuscript review comments by Tien Grauch, A.C. Huffman, Jr., Marilyn A. Grout, Terry Offield, Robert Hite, and Earl R. Verbeek.

## GEOLOGIC SETTING OF THE PARADOX BASIN

The Paradox Basin of southeastern Utah and southwestern Colorado is an intracratonic basin of Middle Pennsylvanian age that developed on continental crust—that is, on an enigmatic cratonic block—within the Colorado Plateau physiographic province. It is a northwest-southeast elongate or rhombic, possibly wrench-related pull-apart basin (Stevinson and Baars, 1986; Sloss, 1988, p. 37) that is bounded by thrust faults on the east at the margin of the Uncompahgre uplift. These thrust faults follow the trend of a proto-Uncompahgre tectonic line that may have controlled the northwest alignment of the Paradox Basin and its internal fold and fault belt (Kelley, 1956; Szabo and Wengerd, 1975). The Uncompahgre uplift, a northwest-trending Laramide structure, was, for a time, sufficiently high standing to expose crystalline basement rocks, the erosional debris of which has formed alluvial fans on the east side of Paradox Basin and clastic sediments that interfinger with evaporite deposits (Hite, 1961) of Pennsylvanian age in the basin proper. The present Uncompahgre block represents a rejuvenated segment of the late Paleozoic and early Mesozoic Uncompahgre highland, an element of the ancestral Rocky Mountains (Dane, 1931, 1935; Holmes, 1956; Tweto, 1980; Case, 1991). Upper Triassic and Jurassic rocks unconformably overlie the Proterozoic on its crest (Williams, 1964; Hansen, 1981).

To the north, the Paradox Basin is bounded by generally flat lying Cenozoic rocks of the Roan Plateau, Roan Cliffs, and Book Cliffs. To the northwest, it is bounded by the San Rafael Swell, which was uplifted in Late Cretaceous to early Tertiary time. The Paradox Basin forms a shallow shelf to the southwest. Stevenson and Baars (1986) suggested that the basin may be bounded on the southwest and southeast by northwest- and northeast-striking shear zones. No evidence for such shear zones has, as yet, been reported.

Stratigraphically, the basin fill, an extensive and thick sequence of Phanerozoic evaporitic, carbonate, and clastic rocks of Pennsylvanian through Quaternary age, overlies crystalline rocks of the Precambrian basement (Williams, 1964; Cashion, 1973).

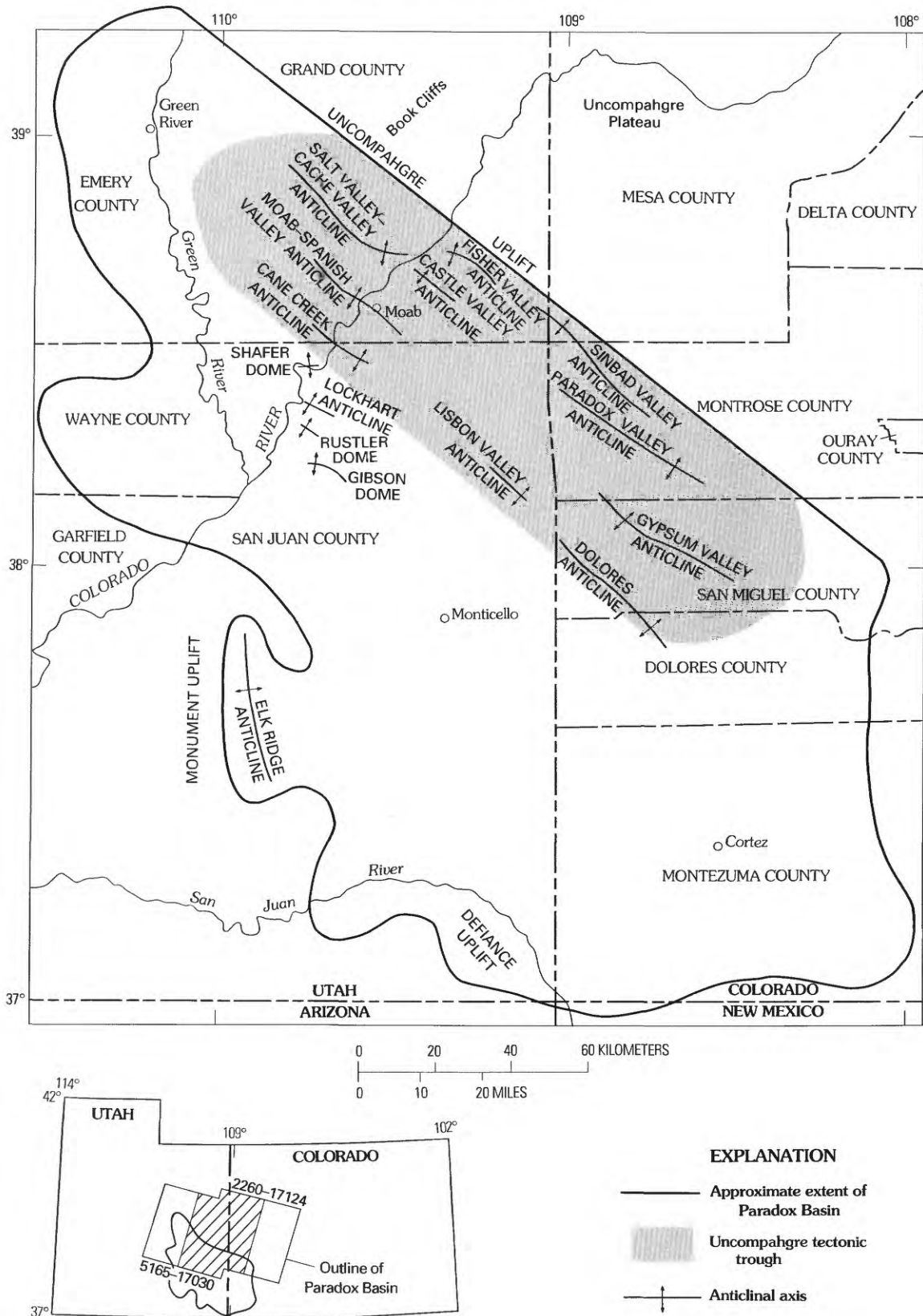


Figure 1. Map showing structural features in area of Paradox Basin, southeastern Utah and southwestern Colorado. Location of Landsat multispectral scanner (MSS) images 5165-17030 and 2260-17124 and area of mapping (diagonal-lined area) are shown in smaller map.

Sandy carbonate and clastic rocks suggest that warping or uplift of the Uncompahgre uplift, which possibly began in Mississippian time, was greatest when the arkosic Cutler Formation of Early Permian age was deposited. At that time major salt flowage within the underlying Paradox Formation resulted in large northwest-striking, parallel salt-cored<sup>1</sup> anticlines. The cores of these anticlines are thickest on the northeast side of the basin.

In the northern part of the area, the Uncompahgre bounding fault is probably a thrust to the southwest (dipping 30° to the northeast). The magnitude of the bounding fault of the Uncompahgre uplift is indicated by the fact that test wells (Frahme, 1984) penetrated 4,540 m (14,000 ft) of thrust Precambrian granite before penetrating fault slices of Mississippian and Devonian rocks overlying beds of the salt-bearing Paradox Formation. These well data suggest that horizontal offset on the Uncompahgre fault is at least 9.7 km (6 mi); vertical offset is about 6,200 m (3.8 mi) (Frahme and Vaughn, 1983). Lineament patterns suggest that the fault trend is close to N. 48°–52° W. Steep and relatively continuous magnetic and gravity gradients along the subsurface Uncompahgre fault zone suggest that the proto-Uncompahgre tectonic line, along which thrusting later occurred, is a fundamental boundary within the Precambrian basement (Cashion and others, 1990).

Stone (1977) placed the first recognizable tectonic activity along the proto-Uncompahgre line in late Precambrian time (Cashion and others, 1990). The resulting faults bounding the proto-Uncompahgre uplift probably determined the trend of the deep-seated northwest-striking faults bounding blocks in the Precambrian basement rocks. The basement blocks in turn controlled the positions and northwest trend of the major salt-cored anticlines of the Paradox Basin (Witkind, 1992).

The surface topography of the great salt-cored anticlines—Salt Valley, Spanish Valley, Castle Valley, Paradox Valley, Fisher Valley, Sinbad Valley, Lisbon Valley, and Gypsum Valley—is characterized by great elongate depressions that form oval valleys over the axes of the salt cores of the anticlines. These valleys have high surrounding walls (Stokes, 1986), complex marginal structures, and salt at shallow depths, in some places beneath exposed gypsum and clastic caprock (for example, in Salt Valley and Fisher Valley) at the valley bottoms.

Tectonic development of the Paradox Basin is characterized by great complexity. One point of view (Stevinson and Baars, 1986) holds that the basin deepened episodically during Middle Pennsylvanian time by rejuvenation of move-

ment along preexisting faults in the Precambrian basement complex, permitting contemporaneous filling with salt 1,830–2,440 m (6,000–8,000 ft) thick. According to this view, pull-apart or wrench tectonism of the basin floor may have triggered salt flowage and diapirism in the eastern, deepest part of the basin; however, the correlation between least principal stress directions and tectonic episodes through time is complex and not yet fully understood. The Antler, Sonoman, Nevadan, and Sevier tectonic episodes, as well as Rio Grande rifting, all resulted in northwest-southeast compression, whereas ancestral Rocky Mountain (manifested here by Uncompahgre thrusting) and Laramide tectonism resulted in northeast-southwest compression, and Gulf of Mexico rifting produced a northwest-southeast least principal horizontal stress (A.C. Huffman, Jr., U.S. Geological Survey, written commun., 1991).

Deformation of the thick salt deposits occurred during the sequence of tectonic episodes and resulted in halokinetic and neotectonic processes that continue to the present day. The extent of the tectonic effect of inherited and nonhalokinetic processes is one of the subjects we address in this chapter. Piercement and nonpiercement salt anticlinal cores and domes and other circular structures are among the most outstanding manifestations of the halokinetic processes.

Spanish and Fisher Valleys are classic examples of asymmetric, one-sided piercement salt-cored anticlines. In Spanish Valley, the major Moab fault zone (Doelling, 1985) along the valley wall juxtaposes Jurassic stratigraphic units against the Cutler Formation of Permian age, indicating that some movement along the Moab fault occurred in Jurassic time or later. This structural interpretation brings a major listric fault to the surface and is compatible with proprietary seismic data (Lee Fairchild, Exxon Production Research Company, written commun., 1990). The Moab listric fault may be a detachment structure controlled in position by subsidence of the salt units of the Paradox Formation and by downdropped graben blocks between horst blocks. The structural situation in Fisher Valley is similar.

In Castle Valley, many faults at the surface are caused by salt movement, including collapse of a massive block of the Wingate Sandstone of Early Jurassic age (Dubiel, 1989). Here, deformation may be mostly nonpiercement in style. The Cane Creek anticline and Shafer Dome may also represent nonpiercement diapirism.

Geomorphic adjustment of valley floors to the upward diapiric movement in the cores of the anticlines has continued into the Holocene, suggesting that halokinetic processes or diapirism are not yet terminated. Evidence of this geomorphic adjustment is to be found in the relatively rapid rate of valley lowering in the basin. Two examples of the rate of valley lowering are given here, although many other examples are available. (1) In Fisher Valley, 111 m (360 ft) of relief, equivalent to downcutting above the Dolores River since deposition of the Pearlette ash (0.6 Ma), indicates an average valley-lowering rate of 0.019 cm/yr. (2) In Spanish Valley,

<sup>1</sup>Although the cores of the anticlines are formed of salt and other evaporites of the Paradox Formation, it is important to recognize that the structure of the folds is significantly influenced by the clastic sedimentary rocks that form the flanks and, in places, the caprock of the anticlines; in this we follow Witkind (1992) in referring to the anticlines as salt cored.

260 m (846 ft) of downcutting since deposition of the oldest Pleistocene gravels (1.4 Ma) also indicates an average rate of 0.019 cm/yr or 190 m (618 ft) during the last million years.

The rate of valley lowering since early Pleistocene time may be approximately equivalent to the rate of salt removal from the anticlinal valleys. The present rate of salt removal by the Dolores River from Sinbad, Paradox, and Gypsum Valleys was estimated by Hite and Lohman (1973) at  $257 \times 10^6$  cm<sup>3</sup>/day; the area of the salt cores of the anticlines projected to the surface in Sinbad, Paradox, and Gypsum Valleys is  $332 \times 10^{10}$  cm<sup>2</sup> (including some areas of exposed Mancos Shale). We infer from these estimates that 282 m (918 ft) of valley lowering has occurred during the last million years as a result of salt removal. Even if this rate is somewhat high for all of Pleistocene and Holocene time, the solution and removal of salt from the anticlinal valleys clearly could account for many halokinetic and neotectonic processes and structures, including linear and circular subsidence structures, in the Paradox Basin. It is also plausible that salt-solution processes are differentially concentrated in areas where faults, joints, and other fractures provide channels of access to the salt cores of both anticlines and circular diapiric structures, resulting in what appear to be negative analogs of diapirism.

Igneous and magmatic activity in Paradox Basin resulted in the laccolith complex of the La Sal Mountains and related stocks(?) and pipes of vent breccia. Similar laccolith complexes are present farther south in the Paradox Basin (the Abajo Mountains) and elsewhere in southeastern Utah (the Henry Mountains and other complexes). Syenite, monzonite, and diorite porphyries are common rock types. The activity at the La Sal complex was dated by Stern and others (1965) at 26–23 Ma and by Stone (1977) at 28–23 Ma. More recent work on fission-track and argon isotope ages for the Abajo, Henry, and La Sal Mountains shows that these laccolithic centers were emplaced between about 30 and 20 Ma in mid-Oligocene to early Miocene time, making them contemporaneous with the Reno-Marysvale and San Juan volcanic zones to the west and east (Sullivan and others, 1991; Nelson, Heitzler, and Davidson, 1992). Interestingly, the La Sal Mountains laccolith complex divides the Paradox Valley-Castle Valley anticlinal structure in two, possibly at the intersection of throughgoing northeast structural trends within the Precambrian basement (Case and others, 1963). If so, the La Sal intrusive activity occurred at a nodal point on the intersection of major northwest and northeast tectonic trends, perhaps in consonance with the distribution of the Abajo Mountains, Henry Mountains, and other laccolith complexes in southeastern Utah. Examination of this question constitutes one of the topics of the lineament analysis presented in the following discussion but requires a more extensive regional investigation as well. On the basis of geologic relations, the times of intrusion of the laccolith complexes of southeastern Utah may have been approximately the same as that of the La Sal intrusions (Hayden, 1877,

Shoemaker, 1956a, and many authors in between). Recent isotope dating (Sullivan and others, 1991; Nelson, Heitzler, and Davidson, 1992a; Nelson, Sullivan, and Davidson, 1992b) indicates 30–20-Ma ages of emplacement.

## SOURCES OF DATA

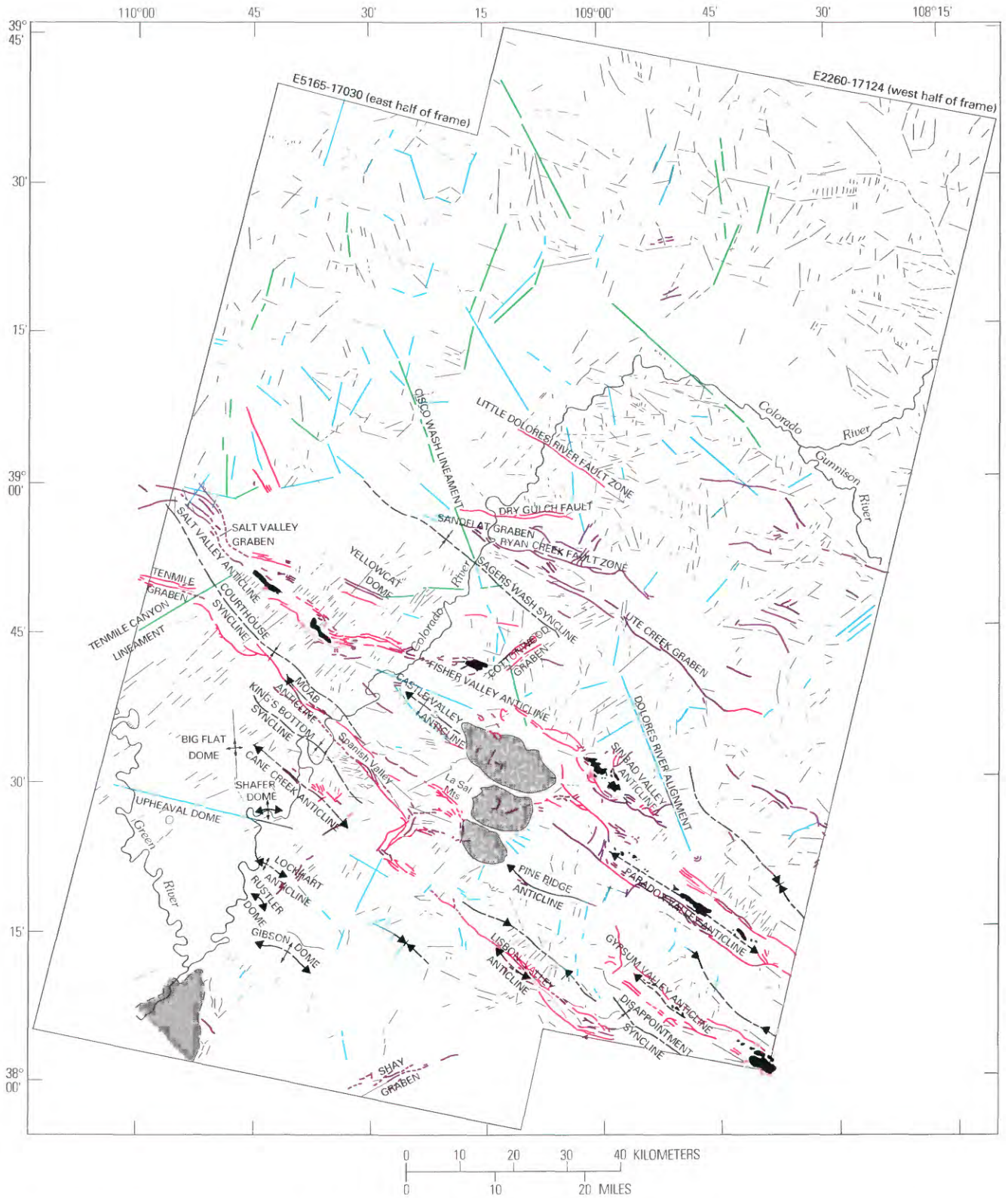
Several types of primary data sources were used for identification, mapping, and statistical analysis of lineaments of the northern Paradox Basin: (1) Landsat multispectral scanner (MSS) images 2260–17124 and 5165–17030 acquired in the early 1970's; (2) uncontrolled X-band radar-mosaic data described in Friedman and Heller (this volume); (3) aeromagnetic and gravity data from aeromagnetic surveys flown by the U.S. Geological Survey between 1953 and 1956 along east-west traverses generally spaced 1.6 km (1 mi) apart and reported by Case and others (1963), Case and Joesting (1973), and Hildenbrand and Kucks (1983); and (4) geologic maps, most published by the U.S. Geological Survey for mapped faults and fold axes (summarized by Williams, 1964, and Cashion, 1973, for the Moab and Grand Junction 1°×2° quadrangles, respectively). More detailed geologic maps are also cited in the text and figures of this report; the geologic map of the Arches National Park by Doelling (1985) was also used, as were geologic field and aircraft observations and handheld photographs by Jules D. Friedman, assisted in field investigations in the late 1970's and early 1980's by Dennis O'Leary and Jack A. Friedman. The senior author was also accompanied in the field on several separate occasions by Robert J. Hite and Eugene M. Shoemaker. Identification and mapping of lineaments and their classification was done by Jules D. Friedman, assisted by Shirley L. Simpson. Data on joint sets between Salt Valley and Deadhorse Point were obtained during field investigations by Jules D. Friedman and much amplified by field data from Marilyn A. Grout and Earl R. Verbeek.

Azimuthal trends of linear features of the Paradox Basin that are taken from the geologic literature and identified and cited in the text and figures are used for comparative purposes.

## DEFINITIONS AND CATEGORIES OF LINEAMENTS AND ALIGNMENTS

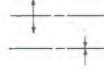
### MAPPED FROM LANDSAT MULTISPECTRAL SCANNER IMAGES

The definition of lineament as used in this investigation is that of O'Leary and others (1976), based on usage introduced and amplified by Hobbs (1904, 1912). "A lineament is a mappable, simple or composite linear feature of a surface, whose parts are aligned in a rectilinear or slightly curvilinear relationship and which differs distinctly from the



**Figure 2 (above and facing column).** Map showing tectonic features in northern part of Paradox Basin, southeastern Utah and southeastern Colorado. Landsat multispectral scanner images 5165–17030 and 2260–17124 were used to map some lineaments and alignments. Modified from Friedman and Simpson (1978, 1980).

## EXPLANATION

-  Landsat lineament coinciding with mapped fault
-  Mapped fault (Williams, 1964; Cashion, 1973)
-  Concealed or inferred fault (Williams, 1964)
-  Landsat lineament connecting mapped fault segments or projection of mapped fault
-  Fold axis (Williams, 1964; Elston and Shoemaker, 1961); dashed where inferred from geologic mapping or Landsat images
-  Major lineament from Landsat images, not previously mapped and generally more than 20 km (12.4 miles) long
-  Lineament from Landsat images
-  Alignment from Landsat images
-  Outcrop of caprock of Paradox Member of the Hermosa Formation (modified from Elston and Shoemaker, 1961)
-  Intrusive dome contact, based on Landsat image
-  Needles fault zone

surface phenomenon." The likelihood that a linear feature mapped from Landsat multispectral scanner images has a subsurface expression is suggested by spatial coincidence with geologically and geophysically mapped structures or by morphology of the linear feature (for example, rectilinearity, distinctness, continuity, tonal contrasts on images, stratigraphic or lithologic offset relations, topographic offsets, and rectilinear geomorphic features including alignments of drainage and landforms).

The plotted lineaments of the Paradox Basin (fig. 2) may be listed in descending order of reliability.

1. Lineaments that coincide with mapped faults.
2. Lineaments that connect segments of mapped faults.
3. Lineaments that coincide with concealed or inferred faults.
4. Lineaments mapped on the basis of rectilinear landform boundaries or tonal contrasts longer than 20 km (12.4 mi).
5. Alignments of short lineaments.

## GEOPHYSICAL LINEAMENTS

The gravity and magnetic lineaments from which azimuthal trends were determined statistically were mapped by Case in the present investigation (figs. 3, 4), according to a method similar to that effectively utilized by Plescia and Heney (1982, p. 211–212) and Frost (1977, p. 353). In this method, gravity and magnetic lineaments constitute linear alignments of contour features including straight-line contour patterns that have a steep gradient relative to surrounding gradients, alignments of maxima and minima, and

alignment of flattened terminations of maxima and minima, or various combinations of these features.

## ANALYSIS OF DATA

The first step in analysis of linear features was to apply the definitions of lineaments and alignments, as given in the preceding section (and in the explanation of fig. 2), to Landsat multispectral scanner (MSS) images. The linear features were mapped in a descending order of subjective reliability at a scale of 1:250,000 to fit the Moab and Grand Junction 1°×2° quadrangles. Descending order of subjective reliability is used here to mean, for example, that a linear feature observed and mapped from a satellite image and that coincides spatially with a geologically mapped fault has a higher likelihood of representing a defined structure than does a linear feature that is not so rigorously constrained. Alignments are given the lowest category of reliability because they represent linear alignments of possibly related but disparate geological features. Their reliability cannot be readily determined. Alignments may, however, represent significant structures at depth and hence are mapped and analyzed separately from other categories of linear features.

The different categories of linear features were analyzed separately by category for strike frequency distribution by 1° azimuthal sectors using the LINANL programs of D.L. Sawatzky (U.S. Geological Survey, written commun., 1981), in a technique similar to that described by Sawatzky and Raines (1981). Linear features from magnetic and gravity field maps were treated similarly but separately.

Using a program of G.R. Olhoeft (U.S. Geological Survey, written commun., 1981), the strike frequency distributions of the various categories of lineaments were plotted by 1° azimuthal sectors on rose diagrams (see figs. 7–10, later). In each rose diagram, the distribution of lineaments in any 1° sector is normalized to the sector having the maximum frequency of lineaments in each category.

Concentrations of lineaments in most categories occupy clusters of 1° sectorial intervals, giving wider sectors. Sectorial clusters of intervals were reported as first-, second-, third-, or fourth-order, depending on relative numerical concentration of lineaments for each of several rose diagrams. First-order clusters have the highest confidence levels within individual rose diagrams, implying that first-order frequency distributions are least likely to be random. Although subjective, first- through fourth-order distributions are all likely to be nonrandom.

When cumulative frequency distributions for several different lineament types are compared, several generalizations emerge.

1. The first-order frequency distribution of major lineaments (that is, those longer than 20 km (12.4 mi) (fig. 7B)

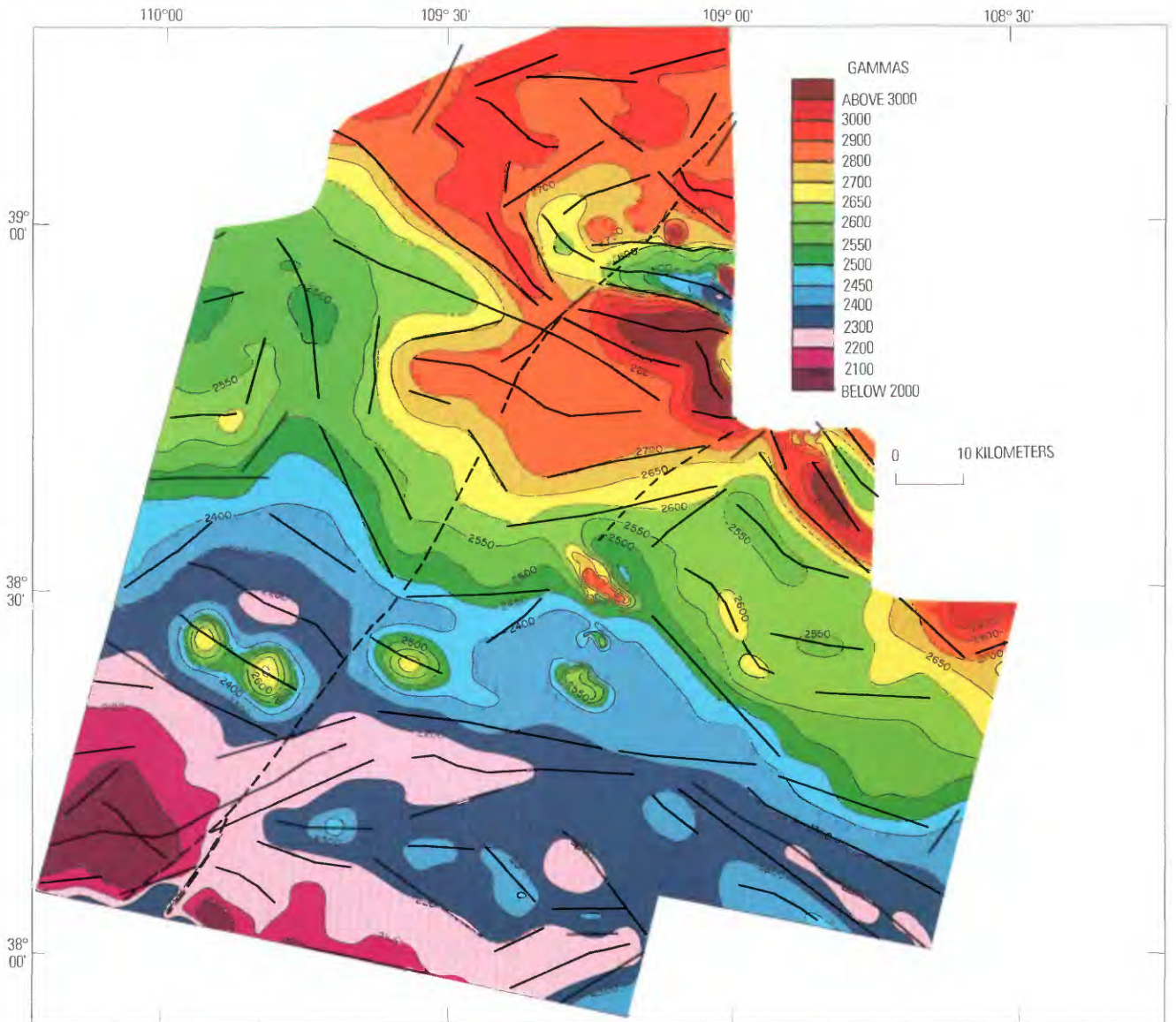


**Figure 3.** Aeromagnetic map of northern part of Paradox Basin, southeastern Utah and southwestern Colorado, showing magnetic lineaments (heavy lines, dashed where queried).

is concentrated between N. 40° W. and N. 60° W. This distribution coincides with the first-order mapped fault distribution at N. 40°–60° W., the first-order magnetic-field lineament distribution at N. 50°–60° W., and the first-order gravity-field lineament distribution at N. 40°–60° W. (fig. 10E).

2. The second-order frequency distribution of magnetic-field lineaments (fig. 9B) at N. 60°–83° W. generally coincides with the third-order frequency distribution of total, non-length-weighted lineaments at N. 67°–78° W. and with a spike in fault distribution frequency at N. 72°–75° W.

3. A spike in mapped fault frequency distribution at N. 40°–50° E. is mostly coincident with or overlaps second-order gravity-field lineament trends at N. 35°–53° E. and

third-order magnetic-field lineament trends at N. 35°–62° E. First-order joint trends between Salt Valley and Deadhorse Point also are at N. 32°–38° E.

4. Joint concentrations at N. 30°–50° E. (fig. 10C) are normal to the trend (N. 40°–60° W.) of surface faults parallel to the axes of salt-cored anticlines (the first-order fault trends), in accord with the observations of Doelling (1985) that at least one set of prominent joints that formed in the Entrada Sandstone (and other units) on the flanks of the collapsing anticlinal crests is at right angles to the faults bounding the subsidence structures. It should be noted here that there are many joint sets in the Paradox Basin; for example, at least six in Jurassic rocks alone (Doelling, 1985; M.A. Grout, written commun., 1992).

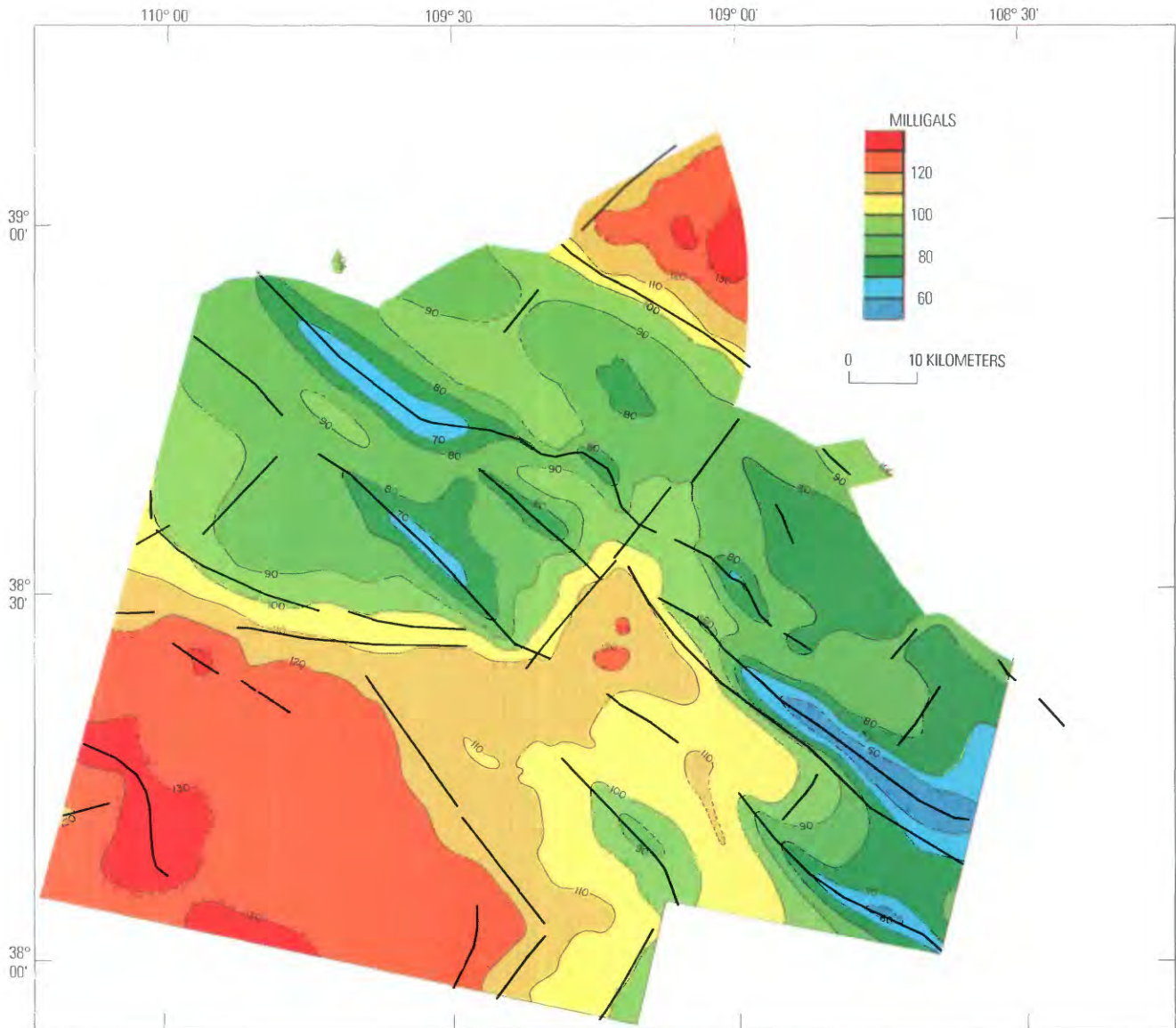


**Figure 4.** Gravity map of northern part of Paradox Basin, southeastern Utah and southwestern Colorado, showing gravity lineaments (heavy lines).

## EVIDENCE FOR PRECAMBRIAN BASEMENT INVOLVEMENT IN NORTHEAST- AND NORTHWEST- TRENDING STRUCTURES IN THE PARADOX BASIN

### REVIEW OF GEOLOGIC AND GEOPHYSICAL EVIDENCE FOR NORTHWEST-TRENDING STRUCTURES

A rose-diagram analysis of first-order fracture patterns in mountain uplifts of the Colorado Plateau is given by

Badgley (1962) (figs. 5, 6) and is repeated here in review of the literature. Each rose represents the summation of several thousand fracture-trend observations. It is not clear whether these summations are predominantly of ground observations or photo interpretations, but they probably include both. Moreover, it is not known over what sectorial sector rounding or averaging was carried out, and we do not know the geographic boundaries of the areas investigated. For these reasons, we make no specific comparisons between these diagrams and those constructed for the current investigation.

Many of the northwesterly structures are clearly exposed at the surface. It is sufficient to state in this section, in review of the geophysical literature, that the strong N. 40°–60° W. strike of faults, joints, and fold axes

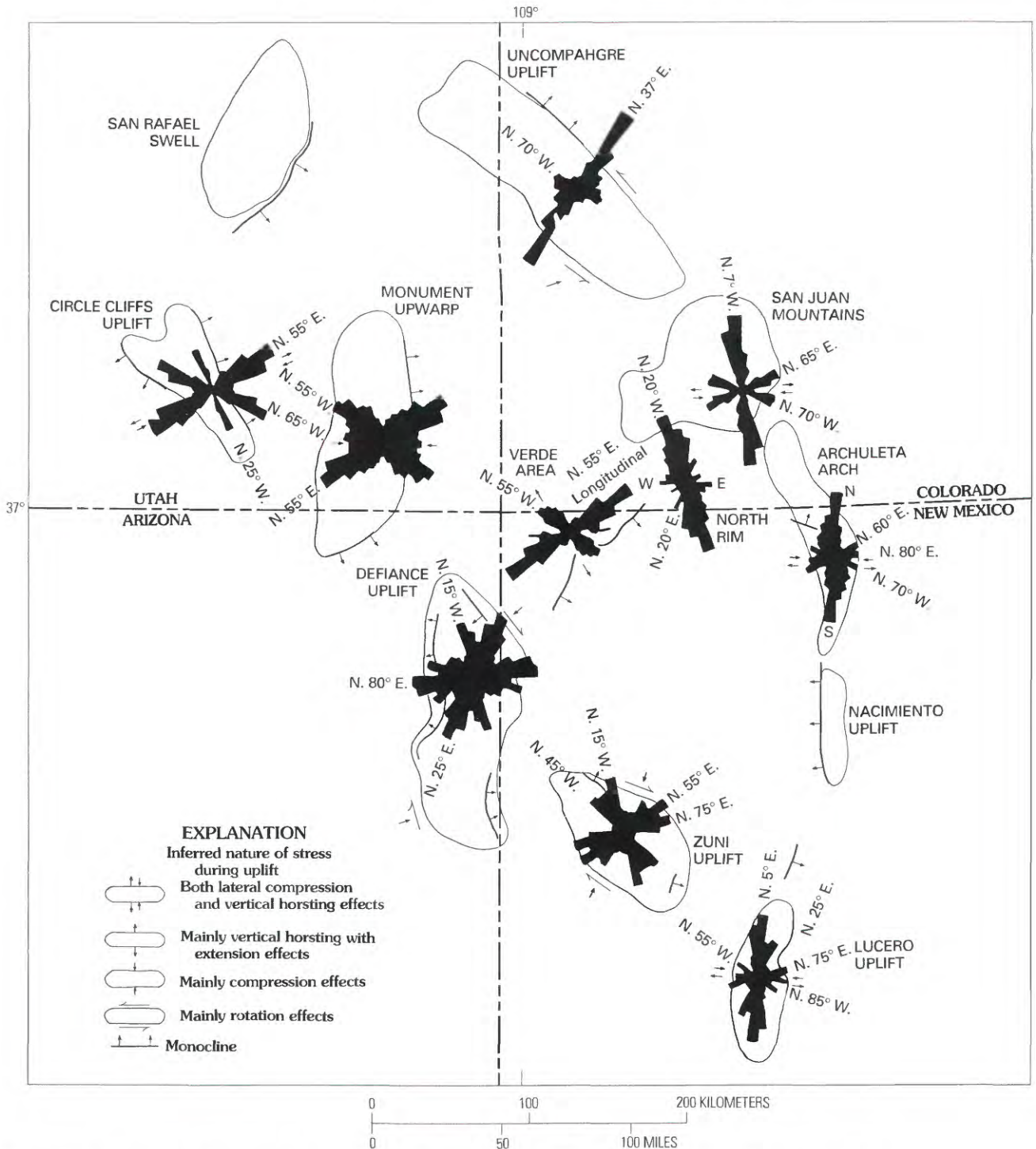
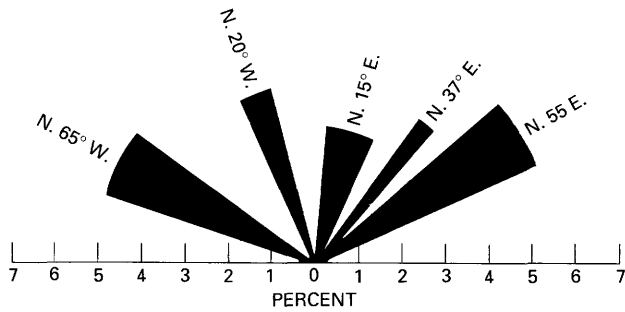


Figure 5. Map showing first-order fracture patterns in area of Colorado Plateau. Modified from Badgley (1962).

coincides almost perfectly with first-order trends in both the gravity and magnetic fields. Many of the magnetic-field trends have been interpreted as representing discontinuities in the basement complex, outlining tilted horst blocks bounded by faults in Precambrian crystalline rocks. These hypothetical blocks and bounding faults may

have controlled emplacement of elongate salt diapir cores of the anticlinal valleys (Case and others, 1963; Case and Joesting, 1973). Stokes (1948) and Eardley (1951, p. 401) noted that the trend of the anticlines, parallel to the northwesterly trends cited above, is also parallel to that of the Uncompahgre boundary fault; Stokes suggested that this



**Figure 6.** Diagram showing fracture orientations in area of Colorado Plateau. More than 10,000 observations are included. Modified from Badgley (1962).

relation points to a system of deep-seated breaks in the (Precambrian) basement rocks. Witkind (1992) also emphasized the genetic relationship between the Uncompahgre uplift and the northwest trend of the major salt-cored anticlines of the Paradox Basin. We note here that the geophysical evidence for deep-seated breaks in the Precambrian basement could also be interpreted, alternatively, as representing, inclusively, faults in the Precambrian rocks of the basement and parallel antiforms or rumpling of the basement complex in response to clockwise rotation of the craton and the resulting northeast-southwest crustal shortening during Laramide deformation (Hamilton, 1981, 1989). Proprietary seismic data (Lee Fairchild, oral commun., 1991) for the Paradox Valley anticline, however, support the concept of deep-seated fault breaks in the Precambrian basement complex, parallel to and beneath the keels of the salt-cored anticlines.

Additionally, the west-northwest (N. 75°–85° W.) trend of lineaments of the magnetic field (fig. 9B) is parallel to conspicuous west-northwest trends of normal faults (E.R. Verbeek, written commun., 1992) beneath the Piceance Basin (Stone, 1977; Johnson, 1983, p. 70) and could be of the same age.

### GEOLOGIC FIELD MAPPING AND REMOTE-SENSING EVIDENCE FOR NORTHWEST TECTONIC TRENDS

Rose diagrams of lineament trends mapped from Landsat images are shown for the entire mapped area (fig. 7) and for discrete tectonic provinces within the area (fig. 8), including the Uncompahgre Plateau, the region of salt-cored anticlines, the Grand Valley, and the Roan Plateau. Rose diagrams for trends of lineaments of the regional gravity and aeromagnetic fields (fig. 9) and geologically mapped faults, fold axes, and joint sets (fig. 10) are given for comparison. The areas covered by these several data sets are mostly but not entirely coincident.

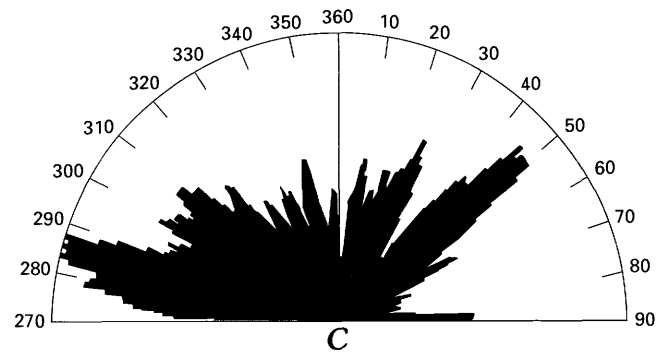
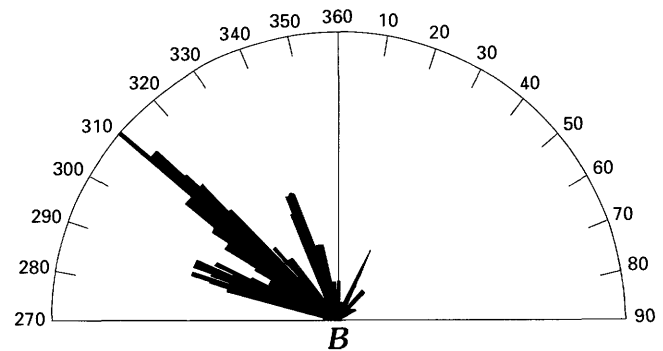
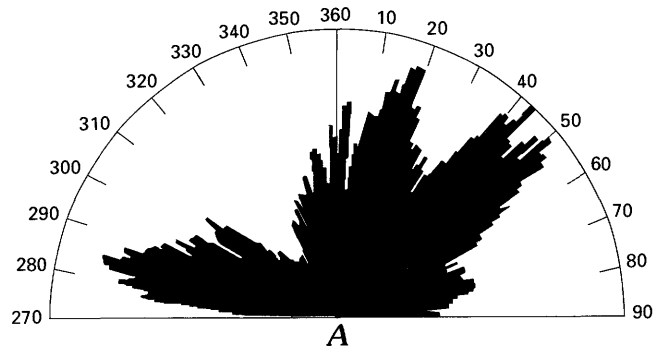


**Figure 7.** Rose diagrams showing frequency distribution of azimuthal trends, as mapped from Landsat multispectral scanner images, for area of northern part of Paradox Basin, southeastern Utah and southwestern Colorado. A, Total lineaments (minus faults); 2,033 lines. B, Major lineaments (longer than 20 km (12.4 mi.); 77 lines, C, Alignments; 254 lines.

The northwesterly lineament trends, as mapped from Landsat multispectral scanner images show two outstanding features. (1) First-order major lineament trends peak at N. 50° W. (fig. 7B), coincident with first-order trends of fold axes (fig. 10A), one set of joints (fig. 10C), and gravity-field trends (N. 44°–56° W., fig. 9A), and are almost coincident with first-order magnetic-field trends (peaking at N. 55°–57° W., fig. 9B) and one of the first-order bimodal peaks of fault strikes (N. 51°–57° W., fig. 10B). (2) On the other hand, if all lineaments are considered (fig. 7A), including very short lines, a third-order peak distribution is at N. 75°–78° W., roughly coincident in azimuth with a low-order modal peak of fault strikes at N. 73°–74° W. (fig.

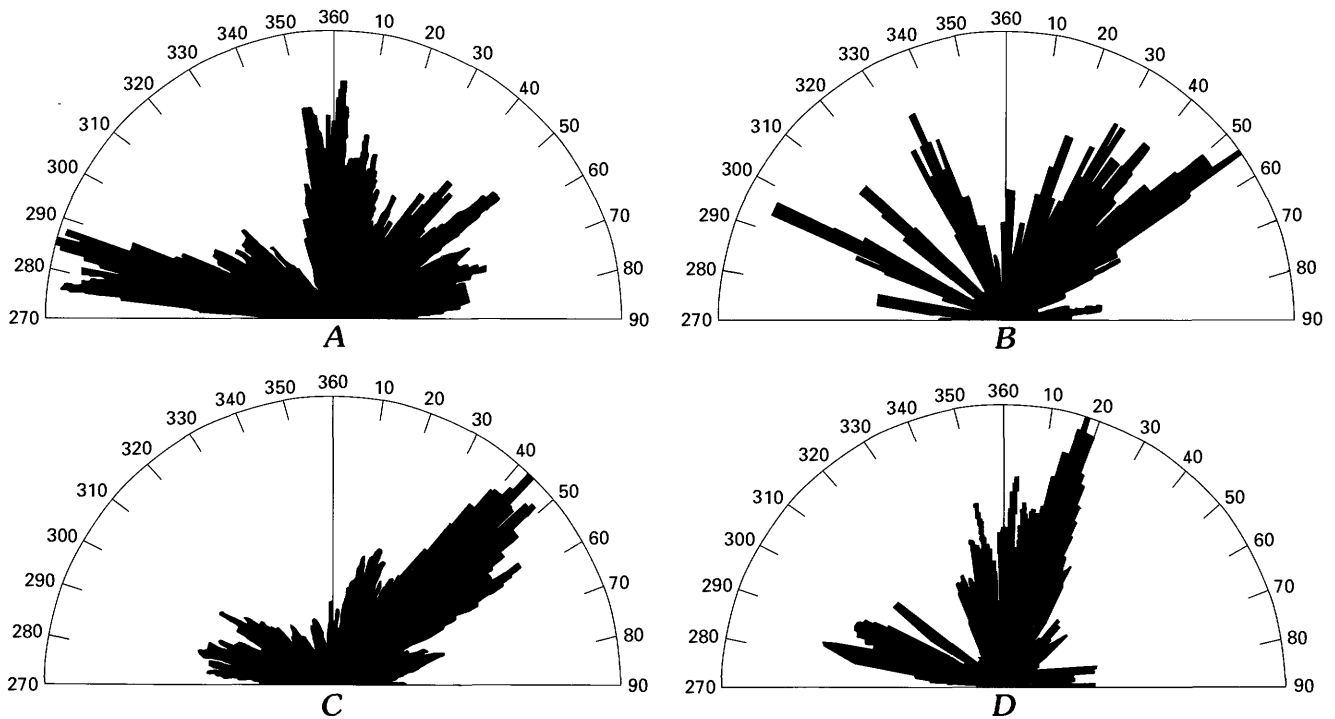


**Figure 8.** Rose diagrams showing frequency distribution of azimuthal trends by tectonic region, as mapped from Landsat multispectral scanner images, for area of northern part of Paradox Basin, southeastern Utah and southwestern Colorado. A, Lineaments of Uncompahgre Plateau province; 478 lines. B, Lineaments of salt anticline province; 801 lines. C, Lineaments of Grand Valley province; 101 lines. D, Lineaments of Roan Plateau province; 606 lines.

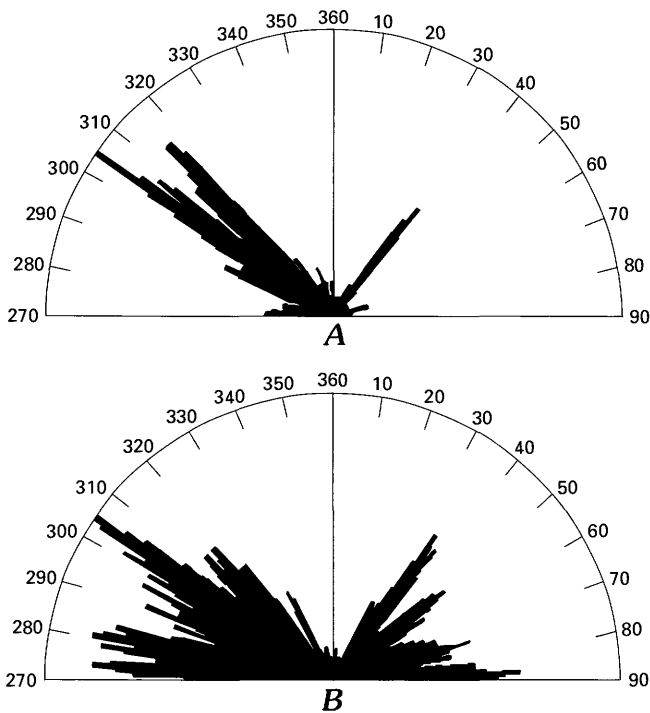


**Figure 9.** Rose diagrams showing frequency distribution of azimuthal trends, as derived from gravity-field and aeromagnetic maps, for area of northern part of Paradox Basin, southeastern Utah and southwestern Colorado. A, Gravity-field lineaments; 89 lines. B, Magnetic-field lineaments; 281 lines.

10B) and a third-order peak of fault strikes within the Moab and Lisbon Valley fault systems (fig. 10D). Perhaps significantly, the dominant (N. 75°–78° W.) northwesterly lineament distribution coincides with a N. 78°–80° W. modal peak in the magnetic field (fig. 9B).

The two modes represented by the northwesterly lineament trends may thus represent two fault or joint systems. The N. 70°–80° W. trend is present south of the thickest salt deposits and at least as far south as the Cane Creek anticline, Lockhart Basin, Gibson Dome, and Harts Draw. The west-northwest trend is also shown in the joint sets. It is younger than the north-northwest and northwest joints and older than the northeast and north-northeast joints in Jurassic and younger rocks, as well as in Triassic and Permian rocks, at least in the Shafer Dome-Cane Creek area. There are even older sets, some of which are north-northeast (M.A. Grout, written commun., 1992).

The higher angle northwesterly lineament trends are approximately parallel to major structures and fold axes and are almost parallel to the important southwestern boundary fault of the Uncompahgre uplift.

Specifically, one of the strongest correlations in the northwest azimuthal quadrant is between the peak at N. 55° W. in the magnetic-field data (and, coincidentally, also in the gravity-field data) and the sharply defined N. 50° W. peak in major thoroughgoing lineaments (more than 20 km long). These peaks also coincide with the

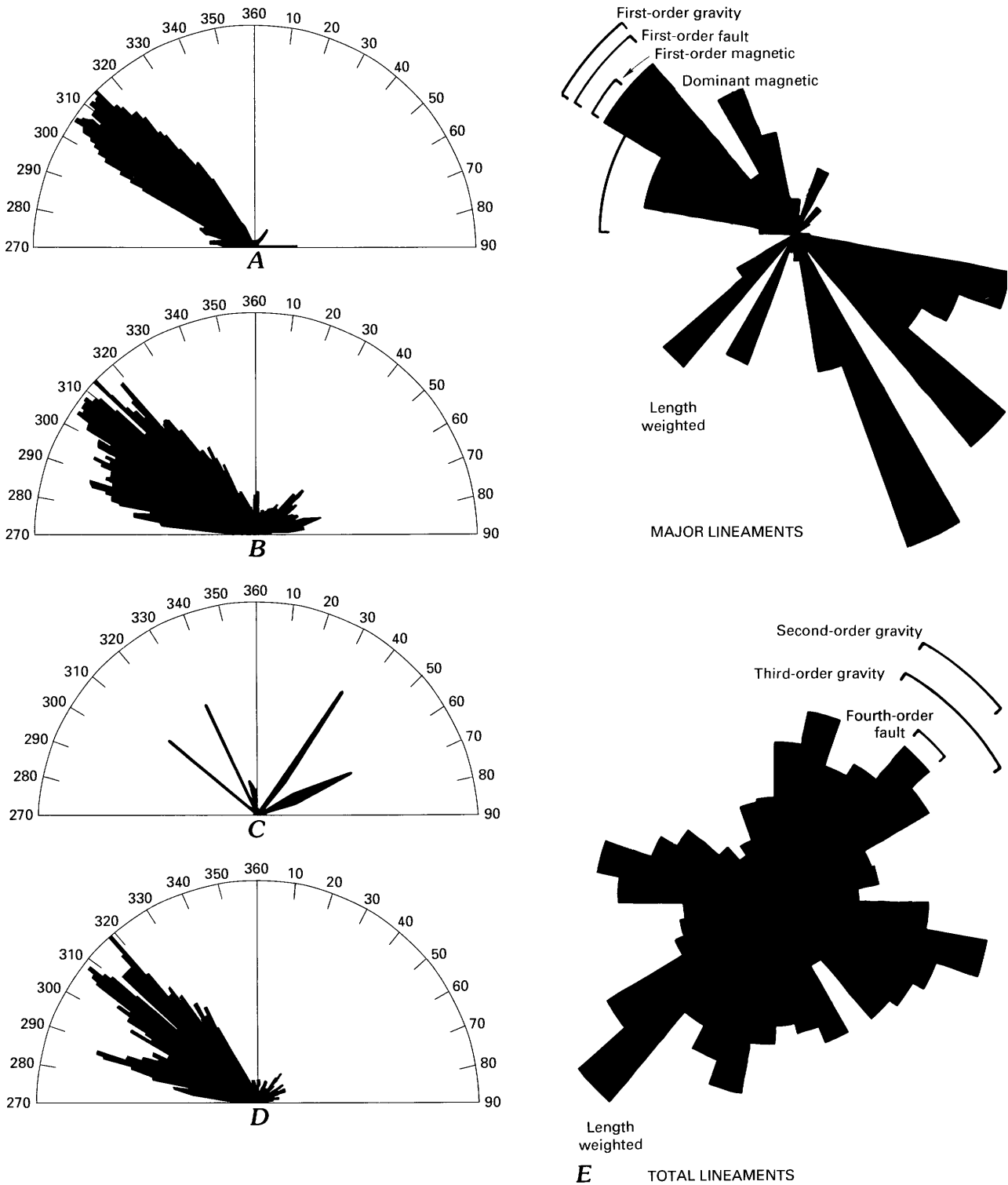


**Figure 10.** Rose diagrams showing frequency distribution of azimuthal trends of joint sets and geologically mapped faults and folds for northern part of Paradox Basin, southeastern Utah and southwestern Colorado. *A*, Fold axes; 176 lines. *B*, Geologically mapped faults; 966 lines. *C*, Joint sets between Salt Valley and Deadhorse Point. *D*, Faults of Moab and Lisbon Valley systems; 209 lines. *E*, Composite rose diagrams showing relation of major lineaments (longer than 20 km, 12.4 mi) (77 observations) and total lineaments (2,033 observations) to azimuthal trends of magnetic (281 lines) and gravity (89 lines) lineaments.

N. 50°–58° W. peak distribution of geologically mapped faults. Because the magnetic field gives the best representation of Precambrian basement structures, the coincidence with long lineaments at the surface, as well as with geologically mapped structures, is strong evidence for some form of structural control of faulting through a multi-stage process in which the proto-Uncompahgre tectonic line controlled the azimuth and position of fault blocks in the Precambrian basement. The fault blocks controlled the localizations of the salt-cored anticlines in post-Mississippian time, and solution and subsidence of the salt in the area of the thickest part of the anticlinal cores caused extensional or subsidence faulting along a northwest trend in the overlying, mostly Mesozoic sedimentary-rock sequence.

### REVIEW OF GEOLOGIC AND GEOPHYSICAL EVIDENCE FOR NORTHEAST-TRENDING STRUCTURES

Salient factors reported in the literature that support the concept of deep-seated northeast-trending structures in the Paradox Basin include the following.

*Structural control of the southwest segment of the Colorado River valley and canyon from the Great Bend west of Grand Junction through Canyonlands.*—Basement fault control of the Colorado River drainage was hypothesized by Mutschler and Hite (1969) to have been significant in the development of the northeast-trending Meander anticline. On the basis of lineament mapping (fig. 2), the entire southwest-trending segment of the Colorado River valley, from the Great Bend west of Grand Junction through Canyonlands, is structurally controlled (Friedman and Simpson, 1978, fig. 6) across the Paradox Basin. Moreover, Wong and others (1987) reported the occurrence of 989 microearthquakes in a northeast-trending zone between 1979 and 1985 that had Richter magnitudes as high as 3.3 and were concentrated along a stretch of the Colorado River from the confluence of the Green River northeast to Moab. The events generally originated in the upper crust. The seismicity probably was the result of strike-slip and normal faulting on preexisting faults that have been reactivated in the contemporary extensional tectonic stress field of the Colorado Plateau (Wong and others, 1987, p. 51).

*A major northeast-trending discontinuity in the basement complex.*—In early geophysical potential-field investigations of Paradox Basin, Case and Joesting (1973, pl. 3, fig. 10) inferred a major northeast-trending fault zone in the basement complex extending northeast from the semiconcentric Needles fault zone to the Little Dolores fault (Williams, 1964). The fault zone inferred by Case and Joesting (1973, A–A', fig. 10) might have offset (B–B', fig. 10) highly magnetic rocks in the Precambrian basement between Upheaval Dome on the west and Behind the Rocks on the east.

*A major northeast-trending discontinuity in the gravity field.*—Case and Joesting (1973) also mapped a significant northeast-trending discontinuity of the gravity field, termed the Wilson Mesa gravity gradient (fig. 11), which is approximately parallel to the magnetic discontinuity. They interpreted this gradient to represent a step in the basement surface parallel to the northeast-trending Precambrian structural discontinuities inferred from the magnetic field.

*The Colorado lineament zone.*—Warner (1978, p. 164) summarized the geophysical and geologic features of the Colorado lineament zone in stating that,

West and northwest of the La Sal Mountains, a series of linear magnetic trends is aligned northeasterly, parallel to a prominent gravity trend and transverse to the regional Phanerozoic structures (Case and others, 1963). The anomalies are interpreted to relate to a structural discontinuity in the underlying basement, probably a fault. Within the anomaly zone, northeast-trending faults break the Mesozoic cover and could be due to Laramide (age) movement on an ancient basement structure, as demonstrated for the Bright Angel and Mesa Butte fault systems in Arizona.

*Northeast continuation of the Bright Angel and Sinyala fault systems of Arizona.*—Shoemaker and others (1978, p. 354) pointed out that where the northeast-trending Bright Angel fault system crosses the Grand Canyon the relationship between the northeast-trending faults and the underlying Precambrian rocks is exposed. Here, the principal displacement of Paleozoic beds along the Bright Angel and parallel fault systems such as the Sinyala fault was controlled by more ancient faults in the underlying Precambrian rocks. Shoemaker and others (1978) concluded that these northeast-trending fault systems in northern Arizona reflect fault zones of major displacement in the crystalline basement and pointed out that they are represented in the Earth's magnetic and gravity fields and can be traced as lineaments on Landsat multispectral scanner images for more than 100 km (62 mi) (Shoemaker and others, 1978, p. 343, fig. 15–1). These hypothetical continuations of known northeast-trending fault systems are parallel to high-angle normal faults at the surface that have relatively small offset. Shoemaker and others suggested (as did Hamblin, 1970) that normal faulting in northern Arizona has continued into Holocene time, and, indeed, seismic activity along these fault systems has occurred recently, for example, in 1974 (Shoemaker and others, 1978, p. 364). One of the parallel northeast-trending fault systems of northern Arizona, the ancestral Sinyala fault system (Shoemaker and others, 1978, p. 359, fig. 15–7), probably is a strike continuation of the Paradox Basin structural discontinuities mapped by Case and Joesting (1973) (figs. 3, 4) and included in the Colorado lineament zone.

*Reactivation of Precambrian fault zones in the crystalline basement rocks of the Marble Plateau, Arizona.*—The fracture network in Permian and Triassic strata of the southern Marble Plateau of north-central Arizona includes a suite of basement-controlled structures that trend about N. 40° W. and N. 50° E. These basement-controlled fractures include both normal and reverse faults that owe their origin to

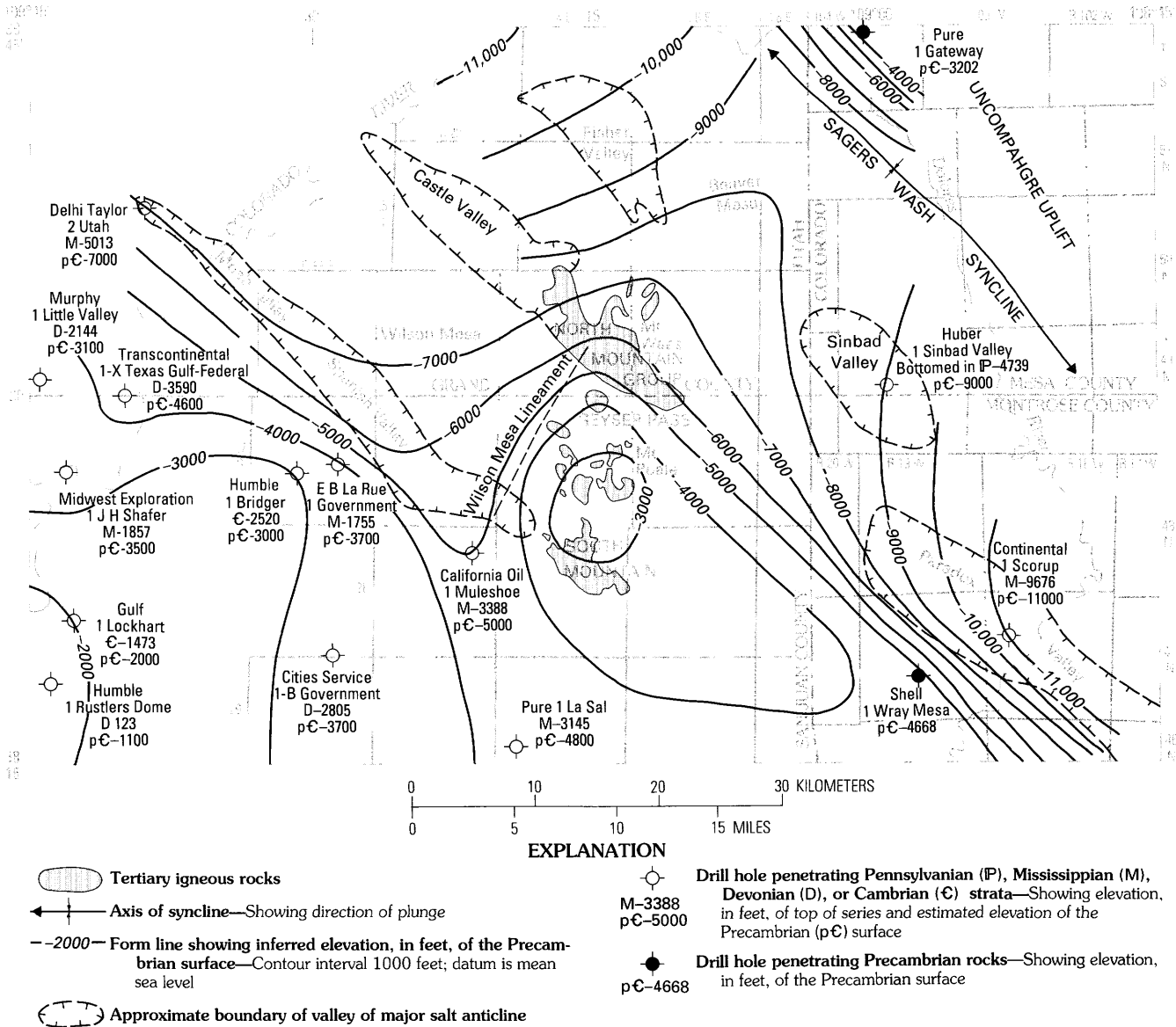


**Figure 11.** Map showing inferred configuration of Precambrian surface in vicinity of the La Sal Mountains, Utah. Location of structure contours is approximate. Modified from Case and others (1963, pl. 3).

episodic reactivation in Laramide time of Precambrian fault zones in the crystalline basement rocks (Sutphin and Wenrich, 1988). More shallow seated, post-Laramide normal faults are widely distributed on the Marble Plateau and were formed by reactivation during shear stress of joint sets striking within  $20^\circ$  of due north (Sutphin and Wenrich, 1988). Each one of these trends is strongly represented in the Paradox Basin.

In a recent review of the tectonic stress field of the continental U.S., Zoback and Zoback (1989, p. 532) concluded that the present-day least horizontal stress direction is northeast-southwest in the Paradox Basin part of the Colorado Plateau. This is compatible with the episode of extensional tectonism that began in Oligocene or Miocene time.

## GEOLOGIC FIELD MAPPING AND REMOTE-SENSING EVIDENCE FOR NORTHEAST TECTONIC TRENDS

The statistically dominant strike frequency of all lineaments mapped from Landsat images of this region (fig. 7A),  $N. 37^\circ\text{--}56^\circ E.$ , shows a first-order bimodal distribution, with peaks at  $N. 44^\circ E.$  and  $N. 52^\circ E.$  A second-order peak is at  $N. 14^\circ\text{--}20^\circ E.$

The first-order lineament distribution is in close coincidence with the second-order gravity-field peak at  $N. 36^\circ\text{--}42^\circ E.$  (fig. 9A), the third-order magnetic-field peak at  $N. 36^\circ\text{--}41^\circ E.$  (fig. 9B), and joints (fig. 10C). The  $N. 52^\circ E.$  lineament peak coincides with a lesser but nonetheless sharp

magnetic peak at N. 49°–52° E. Major alignments (fig. 7C) coincide with the N. 42°–52° E. peak. Fourth-order mapped fault peaks are at N. 46° E. and N. 74° E. (fig. 10B).

The first-order distribution of length-weighted lineaments of the Paradox Basin is at N. 40°–50° E., as is the second-order distribution of alignments. These trends are coincident with the second-order azimuthal distribution of gravity lineaments, third-order distribution of magnetic lineaments, and fourth-order distribution of faults. This trend also coincides with the La Sal Mountains magnetic lineament trend of Johnson (1983) and with the N. 50° E. trend of basement-controlled structures of the Marble Plateau of north-central Arizona interpreted as caused by reactivation of structures of the Precambrian basement in Laramide and post-Laramide time (Sutphin and Wenrich, 1988). The northeast continuations of the Sinyala and Bright Angel fault trends of Shoemaker and others (1978) are closely coincident.

The second-order lineament peak at N. 14° E.–20° E. (fig. 7A) is clearly coincident with one of the youngest joint sets in the Piceance Basin; the joints formed during final uplift of the basin and are 10 million years old or younger (Grout and Verbeek, 1991). In the Marble plateau area of northern Arizona joint sets at N. 10°–15° E. are of post-Laramide age (Sutphin and Wenrich, 1988). In the Paradox Basin this trend is most easily observed in the region of the Green River Formation on the Roan Plateau (fig. 8D), to a lesser extent on the Uncompahgre Plateau (fig. 8A), and in part of the Grand Valley (fig. 8C).

In sum, the northeast-trending lineaments, for the most part, represent (1) northeast-striking joint sets (Friedman and Simpson, 1978, p. 26–28), (2) extensional vertical fractures that have little or no horizontal offset (Hite, 1975), and (3) extensional high-angle faults that have predominantly vertical offset (Weir and Puffett, 1960; Weir and others, 1961; Hinrichs and others, 1968) but are parallel to structural trends of the Precambrian basement complex.

### POSSIBLE INVOLVEMENT OF THE PRECAMBRIAN BASEMENT

The trend of both northeast and northwest lineaments suggests a parallelism between surface structural trends and discontinuities of the Precambrian crystalline basement rocks as delineated in the gravity and magnetic fields (Case and Joesting, 1973, pls. 1–3).

Landsat multispectral scanner images show northwest and northeast fracture trends or lineaments in the Uncompahgre Plateau (fig. 8A) that are compatible with the dominant lineament trends of the entire region of the Paradox Basin (fig. 7A) as shown in the rose diagrams. In the Ryan Creek fault zone (Williams, 1964), for example, geologic mapping shows northeast-striking faults (fig. 12, fault 12) and associated faults and lineaments that cut both

underlying Precambrian crystalline rocks and the overlying Kayenta Formation and Wingate Sandstone of Early Jurassic age. Although the northeast-trending lineaments of the Uncompahgre Plateau depict a seemingly consequent drainage system parallel to the regional slope, it has long been known that basic drainage patterns are influenced by and follow regional structural trends (Bloom, 1978, p. 268–273). We suggest here that the parallel drainage courses of the Uncompahgre Plateau are structurally controlled. Drainage patterns are among the chief surface indications of the trends of joints and faults throughout the Paradox Basin and elsewhere on the Colorado Plateau. As noted by Maarouf (1983), fractures expressed at the ground surface in the early stages of stream history have significantly localized the distribution of drainage lines. Many streams probably initiated their courses as random consequent streams on gently sloping terrain but gradually developed patterns that were increasingly controlled by fracture zones.

Geologic mapping (Hinrichs and others, 1968, 1971) and lineament mapping using Landsat multispectral scanner images (Friedman and Simpson, 1978, 1980) provide substantial evidence of northeast-trending high-angle extensional faults and fractures of post-Paradox age in that part of the Paradox Basin containing diapiric salt-cored anticlines and the thickest salt units. Where the northeast-trending Precambrian structural discontinuities (figs. 10, A, B, section 1c, of Case and Joesting, 1973) pass between Hatch Point and the La Sal Mountains, an en echelon cluster pattern of northeast-striking faults has been mapped in proximity to the surface projection of the Precambrian structural discontinuities. These faults cut Phanerozoic rocks at the surface at the southeast terminus of Spanish Valley (fig. 12, faults 42–48), at the Cane Springs anticline (fig. 12, faults 5, 6), and at Lockhart Basin (fig. 12, faults 1–4). Southwest projections of some of these fault traces appear as lineaments on Landsat multispectral scanner images. Several kilometers to the west, the northeast-striking Roberts rift fracture (figs. 12, 13) mapped by Hite (1975) is parallel to the above-mentioned structures. The most recent time of movement along these structures is post-Paradox Formation, and indeed several fractures including the Roberts rift have alteration zones and contain tectonic breccia of underlying stratigraphic units; for example, the Roberts rift contains breccia fragments of the Hermosa Group (Hite, 1975). One tectonic interpretation of these alteration zones is given in a later section.

One cluster of high-angle northeast-striking faults (fig. 12, faults 1–4 and associated lineaments) of en echelon character northeast of Hatch Point cuts Lockhart Basin. On the basis of stratigraphic cutting relations these faults are post-Kayenta Formation (post-Early Jurassic) in age and may be much younger; they are overlain only by gravels of Quaternary age. They strike N. 40°–54° E., and offset along these faults has been predominantly vertical, although some scissors movement may have occurred. Two high-angle faults here have controlled a downdropped structural block

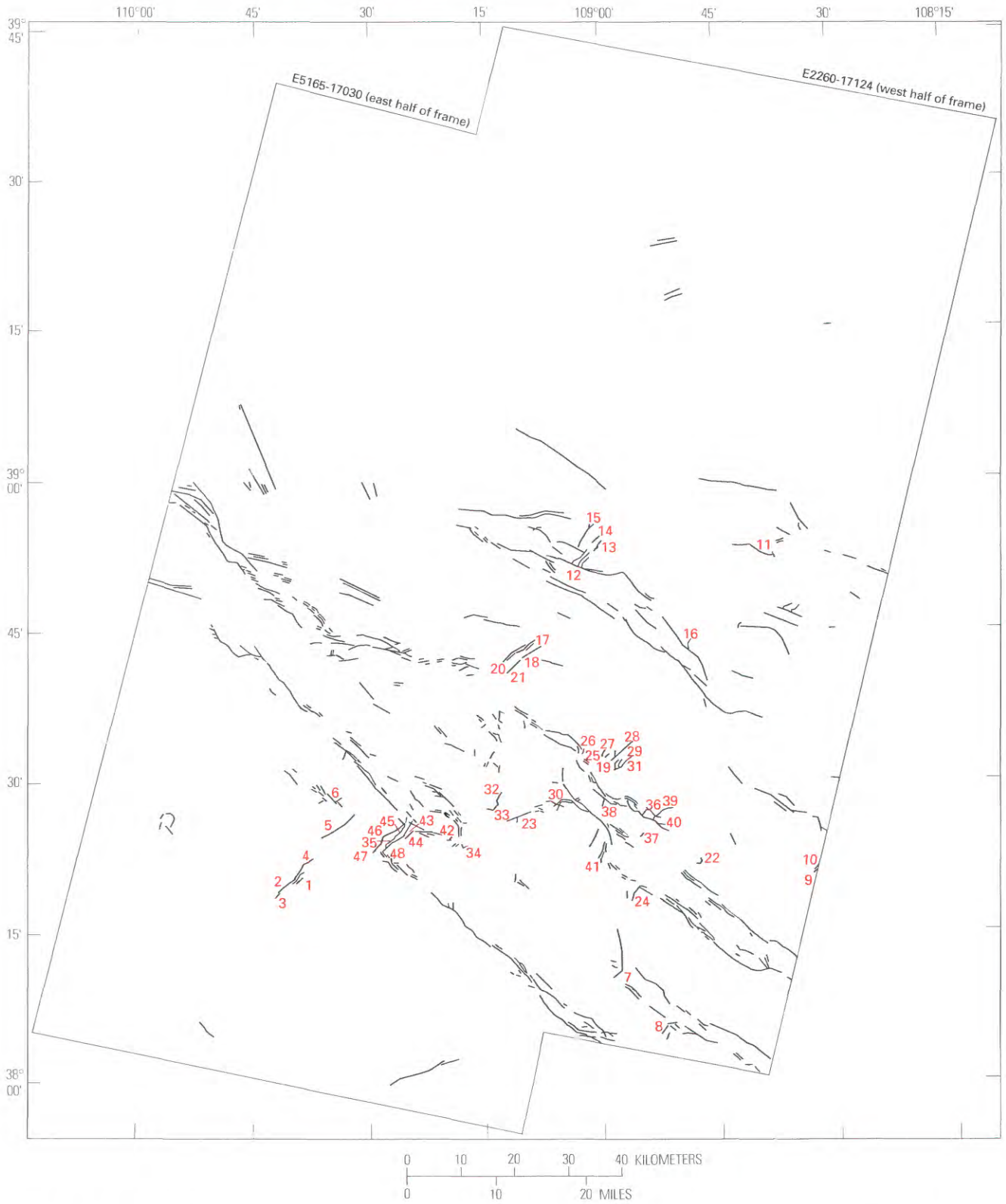


**Figure 12.** Map showing location of mapped and inferred faults in northern part of Paradox Basin, southeastern Utah and southwestern Colorado. Northeast-trending faults are numbered 1 through 48 (see table 1). Modified from Friedman and Simpson (1980).

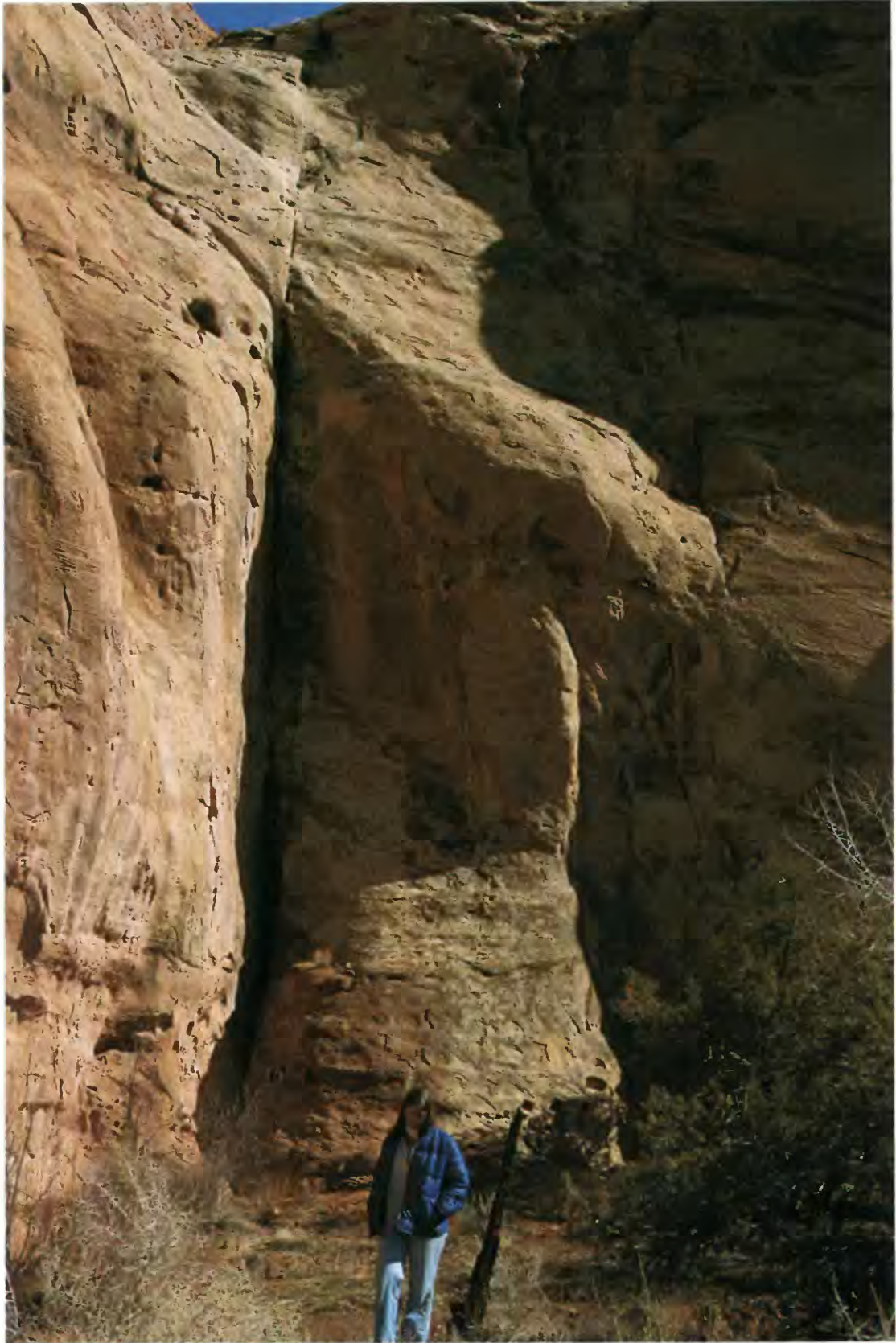


**Figure 13.** Vertical fracture in Roberts rift fault zone, Entrada Sandstone, near Bull Canyon, Moab 1°x2° quadrangle, Utah. Fracture strikes northeast. Photograph by Jules Friedman.

or graben. Structure sections accompanying 1:24,000-scale geologic maps (Hinrichs and others, 1971) allow the inference that some of the faults may cut and offset part of the Hermosa Group. Moreover, the Lockhart Basin fault system is associated with several shallow and deep electrical anomalies (Watts, 1982). Within the 6-km (3.8 mi)-diameter of the circular Lockhart Basin (T.W. Offield, U.S. Geological Survey, written commun., 1983) are several smaller circular collapse features (Huntoon and Richter, 1979; Huntoon, 1982), suggestions of salt seepage to the surface, and the possibility that salt of the Paradox Formation may be missing at depth. Magnetometric resistivity surveys (Fitterman, 1982) confirm that the Lockhart Basin fault system extends to the southwest toward Rustler Dome.

We suggest here that northeast-striking faults in the subsurface provide a linkage between several of these circular, probably halokinetic subsidence structures. Circular subsidence features, as well as intrusive laccolith clusters (including the La Sal Mountains), are at apparent intersections of major northeast- and northwest-striking faults of the basement and at intersections of major lineament systems.

North-northeast of the Lockhart Basin fault system, another cluster of short, high-angle faults and associated northeast-trending lineaments cuts the Cane Creek anticline (Hinrichs and others, 1968). Fault 5 (fig. 12), striking N. 58° E., the most prominent fault in this cluster, cuts and vertically offsets the southeastern, plunging nose of the Cane Creek anticline. Near-parallel northeast-striking faults cut the stratigraphic sequence from the Lower Jurassic Kayenta Formation down to and including the Rico Formation of Middle Pennsylvanian to Early Permian age, the oldest formation mapped at the surface. On the basis of structure sections and structure contours drawn on the base of the Chinle Formation, fault 5 could conceivably offset the diapiric salt core (Paradox Formation) of the Cane Creek anticline. Cutting relations indicate that the time of faulting is post-Navajo Sandstone (post-Early Jurassic) in age. The Cane Creek en echelon fault cluster lies slightly east of the surface projection of the Precambrian structural discontinuity of Case and Joesting (1973).

About 10 km (6 mi) east of the Cane Creek Fault cluster and about 14 km (9 mi) northeast of the Lockhart Basin fault system, another northeast-striking fault cluster (fig. 12, faults 42–48) of en echelon character lies astride another Precambrian structural discontinuity (Case and Joesting, 1973), at the abrupt southeast terminus of the Spanish Valley diapir. This fault cluster, like those of the Lockhart Basin and Cane Creek anticline, consists of many fault segments and lineaments in addition to those shown on figure 12. In the Mount Peale 2° NW quadrangle, Weir and others (1961) mapped high-angle fault 43, which strikes N. 30° E. where it passes between two patches of caliche-cemented alluvial gravels (map unit Qgo of Weir and others, 1961) of early Pleistocene age in the southeast corner of section 30. Fault 43 is overlain by younger alluvial gravels (map unit Qgy of

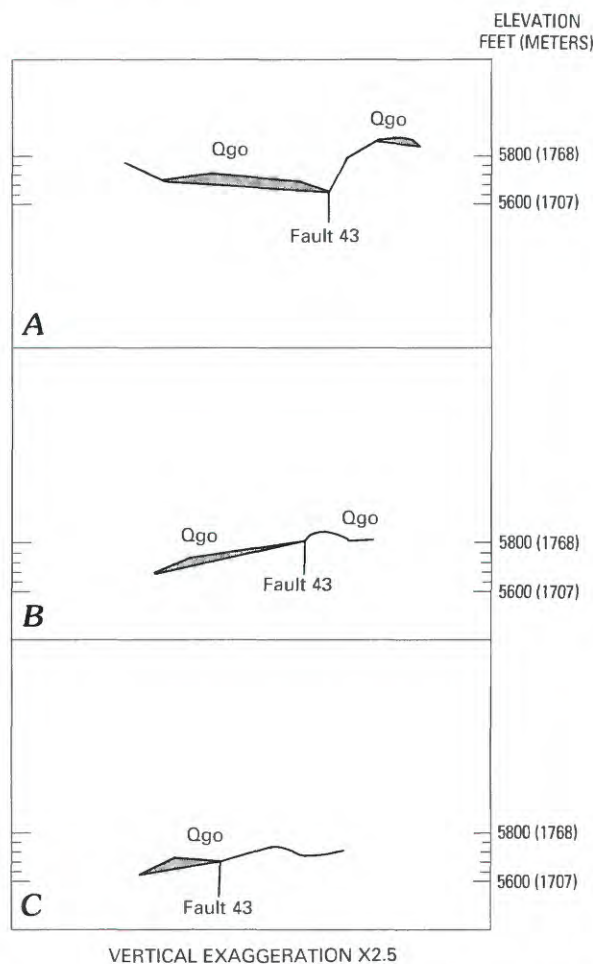


**Figure 14.** Structure sections of fault 43 (fig. 12, table 1), Mt. Peale 2° NW quadrangle (sec. 30), San Juan County, Utah. Section A is northernmost; elevation of sections in feet. Map unit Qgo of Weir and others (1961) is caliche-cemented alluvial of Early Pleistocene age. Modified from Shawe and others (1961).

Weir and others, 1961) of late Pleistocene age. The two patches of unit Qgo probably were eroded away from the fault trace and are separated from each other laterally by more than 124 m (400 ft) and vertically by as much as 67 m (220 ft); it is significant that they are at different elevations and that structure sections (figs. 13, 14) show that the dip of the western patch of unit Qgo is skewed in relation to that of the eastern patch. It is likely that these two patches were originally contiguous and subsequently cut by fault 43 and eroded along the fault line. If so, the time of latest faulting would be bracketed between early and late Pleistocene. Fault traces of this Spanish Valley en echelon cluster appear as northeast lineaments on Landsat multispectral scanner images.

If the depth of penetration of these high-angle faults at the southeast terminus of Spanish Valley is one-half their

strike length, a penetration depth for these structures of about 4,000 m (13,000 ft) could be inferred, but there is no unequivocal evidence that they are that deep. Elston and Shoemaker (1961) showed a +3,000-ft (920 m) contour for the top of the Paradox Formation salt, and the ground surface elevation is about 1,830 m (6,000 ft) at this location; accordingly, the top of the salt would be about 920 m (3,000 ft) deep (R.J. Hite, U.S. Geological Survey, written commun., 1982). Because movement on these high-angle faults was essentially vertical, with a scissors component, offset or penetration of the salt units here is possible. Indeed, on the basis of drill-hole data the salt units are missing or attenuated southeast of the Spanish Valley fault cluster (R.J. Hite, oral commun., 1982).

We note here that normal faulting (that is, near-rigid tectonic deformation) of the salt along these post-Paradox-age faults may not have occurred. It is more likely that halokinetic processes, including flowage of salt under lithostatic stress, did occur and that the northeast-striking faults and other fractures provided access channels both for salt flowage and for movement of groundwater to the anticlinal salt cores. In the vicinity of the Spanish Valley fault cluster, as in Lockhart Basin, Weir and others (1961) have mapped circular collapse structures that suggest subsurface solution and removal of salt. It remains likely that these short northeast-striking normal faults are actually the result of salt solution and subsidence, although their strike trend may be controlled by deeper seated tectonic features.

Further geologic evidence for a relationship between the deep-seated northeast-trending structural discontinuities in the Precambrian basement and surface structures in the Paradox Basin includes the presence of alteration zones along the Roberts rift fracture, previously mentioned, and similar alteration zones along northeast-trending fractures in the northeast wall of the Sinbad Valley structure and elsewhere. These possibly metasomatic alteration zones may have been formed by mobilized brine solutions carrying metallic and sulfide ions upward through fractures deep in the Phanerozoic sequence of redbeds (Hite, 1975). The source of these metal-bearing brines may have been the Paradox Formation, but the less likely possibility of an intrusive or crystalline basement source cannot be ruled out. Copper, uranium, vanadium, and other traces and occurrences of metallic ions along northwest-striking fault zones such as the Lisbon Valley fault lend credence to this possibility. It has long been inferred and often reiterated in the literature of metallic ore deposits that ore occurrences and traces tend to be localized along some major lineaments. In fact, near-surface igneous intrusive bodies such as the La Sal Mountains laccolith cluster and ore minerals emplaced during periods of tectonomagmatic activity tend to be localized along structural zones that coincide with long-lived deep faults (Case and Joesting, 1973, p. 28; see also Khazov, 1980). Further

correlation between metallogenic zones, igneous activity, and deep basement faults manifesting both strike-slip and vertical movement has been inferred in Eurasia. These faults in the East Siberian platform are difficult to map at the surface and were detected by using magnetic, gravimetric, deep-sounding electrical, and seismic methods and by interpretation of satellite images (Yegorov, 1981). That the Paradox Basin Precambrian structural discontinuities evident in the geophysical data represent such a deep fault zone, perhaps reactivated during Phanerozoic time, is similar to the conclusions drawn by Shoemaker and others (1978) for the Bright Angel, Mesa Butte, Sinyala and other fault systems of northern Arizona and is compatible with the conclusions of Sutphin and Wenrich (1988).

It is perhaps more than a coincidence that (1) the Sinyala fault system is on a strike projection with Paradox basement discontinuities,<sup>2</sup> (2) volcanic centers are localized along northeast trends of several northern Arizona deep fault systems (Shoemaker and others, 1978, p. 349), (3) the La Sal Mountains laccolith cluster was emplaced at the intersection of the Paradox Valley-Castle Valley northwest-trending lineament and one of a series of the Paradox Basin northeast-trending structural discontinuities, (4) the La Sal complex was emplaced in mid-Tertiary time—that is, 28–23 Ma (Stern and others, 1961; Stone, 1977; Sullivan, and others, 1991; Nelson, Heizler, and Davidson, 1992; Nelson, Sullivan, and Davidson, 1992)—during or following the period of tectonomagmatic activity represented by the northeast-trending structures of the Paradox Basin, and (5) the long segment of the Colorado River flowing through the Paradox Basin follows a similar northeasterly trend and is probably structurally controlled.

Structural control of drainage is also manifest at Harts Point southeast of Gibson Dome. At least eight parallel, northeast-flowing tributaries to the subsequent stream of Harts Draw have cut canyons on the northeast slope of Harts Point (southwest quadrant of Moab 1°×2° quadrangle). Together with the northeast drainage of North Cottonwood Creek, Lavender Creek, and Davis Canyon, which are tributary to Indian Creek, this entire drainage system forms a modified trellis drainage pattern. The drainage system is complex, combining elements of directional, joint, and parallel fault trellis systems, all of which were included by Bloom (1978, p. 268–272), following the usage of Howard (1967), in the category of structurally controlled landforms. We regard the northeast trends of the Harts Draw tributaries and Davis Canyon, Lavender Canyon, and North Cottonwood Canyon as of special tectonic significance because of

<sup>2</sup>The structural relationship between circular features discovered by use of satellite images and the development of linear fault systems has been outlined by Kosygin and others (1980, p. 1454–1458).



**Figure 15.** Oblique aerial view to northeast across Salt Valley anticline, Moab 1°×2° quadrangle, Utah. Two well-developed joint sets, one striking northeast, are visible in the middle ground on the southwest flank of anticline near Klondike Buttes. These extensional joints in the Entrada Sandstone are of Jurassic age or younger. Photograph by Jules Friedman.

their parallelism to the general Paradox Basin northeasterly lineament trends (fig. 7A) and alignments (fig. 7C) and to the dominant northeasterly lineament trends of the salt-cored anticline tectonic province (fig. 8B). The direction of the subsequent Harts Draw follows the dominant or first-order northwesterly trend of faults and folds of the Paradox Basin (figs. 10A, B) and faults of the Moab and Lisbon Valley fault systems (fig. 10D). The trend of the Harts Draw-Indian Creek drainage and that of the northeast canyon tributaries both follow dominant azimuthal trends of the magnetic (fig. 9B) and gravity (fig. 9A) fields, which mark discontinuities, folds, uplifted blocks (or antiforms), or faults in the underlying crystalline rocks of the Precambrian basement.

At least two inferences from these observations are possible. The first is that the structural pattern of the tectonic province of salt-cored anticlines, involving long northwest-trending faults and fold axes and short northeast-trending extensional faults and joints (figs. 15–17) continues to the southwest to the vicinity of the Indian Creek-Harts Draw

drainage and to the San Rafael Swell on the west, as far as the zero-isolith of the subsurface salt (Baars and Stevinson, 1981; Witkind, 1992). Because the fault (and lineament) set trending N. 40°–60° W. cuts the eastern margin of the San Rafael Swell and the swell was well developed between Late Cretaceous and early Tertiary time (Witkind, 1992) prior to these faults, the N. 40°–60° W. fault set (and lineaments) is probably mid-Tertiary in time of faulting. Because the N. 40°–60° W. fault set is constrained by the zero-isoliths of the underlying salt of the Paradox Formations, the entire fault set is probably the result of solution and subsidence of the underlying salt. The locus and azimuths of the N. 40°–60° W. faults in the clastic rock section overlying the Paradox Formation are likely to have been controlled by the position and boundaries of the block faulting of the Precambrian basement, hence the congruency or coincidence of trends of surface lineaments and lineaments mapped in the magnetic field data. Secondly, circular subsidence and diapiric or intrusive uplift structures such as the Needles fault zone and the La Sal Mountains laccolith complex may be



**Figure 16.** Northeast-trending joint set in the Entrada Sandstone on southwest flank of Salt Valley anticline, Moab 1°×2° quadrangle, Utah. Incipient development of fins occurred across the top of the flexed Entrada Sandstone when salt anticlines formed (Doelling, 1985, p. 13). View looking northeast. Photograph by Jules Friedman.

related indirectly to the development of deep-seated, north-east-trending discontinuities of the Precambrian basement complex. The northeast structural trends controlled the course of the Colorado River in this region and the subsequent erosion of the Phanerozoic sequence.

The river has eroded entirely through the brittle clastic rocks overlying the ductile Paradox Formation, permitting, according to McGill and Stromquist (1979), downdip flow in the Paradox evaporites with consequent extension and faulting within the brittle plate of overlying clastic rocks, producing systematically spaced grabens of the Needles fault zone,<sup>3</sup> which in plan are curved and in direction of dip are concave (McGill and Stromquist, 1979, p. 45–47). The unloading process and lubrication of the top of the salt have thus provided the tectonic setting in which the gravity sliding

hypothesis of Huntoon (1982) is a logical development of the work of McGill and Stromquist for structural evolution of the Needles fault zone.

### TIME OF MOVEMENT AND TECTONIC SIGNIFICANCE OF NORTHEAST-STRIKING FAULTS

Forty-eight northeast-striking faults along which measurable, mostly vertical, displacement has occurred have been mapped by geological methods and are summarized and shown in figures 12 and 18 and table 1. These faults were analyzed for recency of movement on the basis of stratigraphic cutting relations (fig. 18). Most faults tabulated are accompanied by additional, generally shorter, faults parallel to them. Many faults are represented by lineaments mapped on Landsat multispectral scanner images; projections and extensions of many of these faults can be observed on the Landsat and X-band radar images (Friedman and Heller, this

<sup>3</sup>T.W. Offield (written commun., 1983) has also inferred an approximately 8-km (5 mi)-diameter circular feature at the northwest tip of Harts Point in this area and a possible major circular subsidence structure of, which the Needles fault zone represents the eastern concentric half.



**Figure 17.** Fully developed fin topography in top unit of the Entrada Sandstone, Moab 1°X2° quadrangle, Utah, in response to valley development over salt-cored anticlines (Doelling, 1985). Photograph by Jules Friedman.

**Table 1.** Forty-eight northeast-trending faults giving formations cut by faults and earliest age of most recent fault movement, northern part of Paradox Basin, southeastern Utah and southwestern Colorado.

[Faults are shown by number in figs. 12 and 18. Formations are listed using unit symbols as shown on geologic maps cited. Kayenta, Wingate, and Navajo Formations and the entire Glen Canyon Group are now considered to be Early Jurassic in age, although they are shown on the maps cited as generally Triassic]

Fault no.	Formations cut by fault	Age of last movement along fault	USGS map no.	Map source
1	Pc, $\bar{K}c$ , Jw, Jk	Post-Kayenta	I-279	Hackman (1959a)
2	$\bar{K}c$ , Jw, Jk	Post-Kayenta	I-278	Hackman (1959b)
3	Jw, Jk	Post-Kayenta	I-278	Hackman (1959b)
4	Pc, $\bar{K}c$ , Jw, Jk	Post-Kayenta	I-278	Hackman (1959b)
5	Jw, Jk	Post-Kayenta	I-279	Hackman (1959a)
6	Jk	Post-Kayenta	I-279	Hackman (1959a)
7	Jms	Ends at northwest fault cutting Kdb	I-360	Williams (1964)
8	Jw, Jms	Post-Morrison	I-360	Williams (1964)
9	Pc, $\bar{K}c$ , Jw	Post-Wingate	GQ-60	Cater (1955a)
10	Jkw, J $\bar{K}n$ , Jse	Post-Summerville	I-360	Williams (1964)
11	$\bar{K}c$ , Jkw	Post-Kayenta	I-360	Williams (1964)
12	Jkw, J $\bar{K}n$	Post-Navajo; pre-Quaternary	I-360	Williams (1964)
13	$\bar{K}m$ , $\bar{K}c$ , Jkw, Jn	Post-Navajo; pre-Quaternary	I-360	Williams (1964)
14	Jmb	Post-Morrison	I-360	Williams (1964)
15	Jkw	Post-Kayenta (between northwest faults that are post-Burro Canyon)	I-360	Williams (1964)
16	p $\bar{C}$ , $\bar{K}m$ , Jmb	Post-Morrison; pre-Quaternary	I-360	Williams (1964)
17	$\bar{K}m$ , $\bar{K}c$ , Jkw, J $\bar{K}a$ , Jec, Js, Jms	Post-Morrison	GQ-81 I-360	Shoemaker (1955) Williams (1964)
18	$\bar{K}c$ , Jw, Jk, Jn	Post-Navajo	GQ-81	Shoemaker (1955)
19	$\bar{K}c$ , Jn, Jk, Jn, Jec, Js	Post-Navajo	GQ-81	Shoemaker (1955)
20	$\bar{K}mm$ , $\bar{K}mu$ , $\bar{K}c$ , Jw, Jk, Js	Post-Summerville	GQ-81	Shoemaker (1955)
21	Pc, $\bar{K}ml$ , $\bar{K}mm$ , $\bar{K}mu$ , $\bar{K}c$ , Jw, Jn	Post-Navajo; pre-Quaternary	I-360	Williams (1964)
22	Jk, Jm, Jec, Js, Jms	Post-Morrison	GQ-83	Shoemaker (1956b)
23	Jk, Jm	Post-Morrison	I-360	Williams (1964)
24	Jgc, Jm	Post-Morrison	I-360	Williams (1964)

volume), including many segments of the Lockhart Basin fault system. In figure 18, each line shows the time span represented by the stratigraphic section cut by each numbered fault and indicates that the most recent movement cannot be older than the age represented by the termination of the line, which indicates the youngest formation cut by the fault. Dots indicate the presence and age of overlying stratigraphic units that are not cut by a fault; therefore, the fault cannot be younger than the overlying unit. Cutting relations suggest that during Quaternary time at least one fault may have been active (fault 27), in addition to reported Holocene activity in the Needles fault zone (Huntoon, 1982). With the exception of numbered faults terminated by cross faults, many of the numbered faults may have had more recent recurrent movement than that indicated by the chart. The reason for this is that the exact age of overlying Quaternary gravels and alluvium is not known; many of these unconsolidated materials may be of Holocene age, giving permissive ages of recurrent fault movement as recent as 10,000 years or less at the southeast termination of the Spanish Valley diapir.

Cutting relations (fig. 18) also demonstrate that north of the southwestern boundary fault of the Uncompahgre uplift (and thus north of the Paradox salt sequence), in the vicinity of the Ryan Creek fault zone, three mapped high-angle extensional faults of northeast strike cut the Precambrian section and the overlying Triassic and Jurassic rocks. Within the northern Paradox Basin where the salt is thickest, at least two high-angle faults of extensional type and comparable strike cut beds of Triassic and Early Jurassic age. At least 37 similar faults of extensional character cut the Jurassic sequence and at least five cut the Cretaceous sequence. At least two faults cut the Tertiary sequence, and perhaps one cuts beds of Quaternary (probable Pleistocene) age. (The Quaternary ages of fault movement in the Paradox Basin are compatible with the map of Howard and others (1978), on which many northwest- and northeast-striking faults of the Paradox Basin are shown as Quaternary to late Quaternary (last 500,000 years) in age.) The faulting thus occurred sometime from Jurassic through Pleistocene time in the strata between the salt section and the surface. If, as

**Table 1.** Forty-eight northeast-trending faults giving formations cut by faults and earliest age of most recent fault movement, northern part of Paradox Basin, southeastern Utah and southwestern Colorado—Continued.  
[Faults are shown by number in figs. 12 and 18. Formations are listed using unit symbols as shown on geologic maps cited. Kayenta, Wingate, and Navajo Formations and the entire Glen Canyon Group are now considered to be Early Jurassic in age, although they are shown on the maps cited as generally Triassic]

Fault no.	Formations cut by fault	Age of last movement along fault	USGS map no.	Map source
25	Approximately located Jk	Post-Kayenta	GQ-83	Shoemaker (1956b)
26	$\bar{K}ml, \bar{K}mm, \bar{K}c, Jw, Jk$	Post-Kayenta	GQ-83	Shoemaker (1956b)
27	Jecu, Jms, Jmb, Kbc, Km, Ql	Post-Quaternary landslide	MF-139	Carter and others (1958)
28	Jmb, Kbc, Kd, Tp	Post-Tertiary porphyry	MF-140	Carter and Gualtieri (1958)
29	Jw, Jk	Post-Kayenta	I-180	Tolbert (1956)
30	Jm, Jw, Jk, Jn, Kbc	Post-Burro Canyon	I-360	Williams (1964)
31	$\bar{K}m, Jeu, Je, Jem, Jms$	Post-Morrison	MF-152	Weir and others (1961)
32	$\bar{K}c, Jw, Jk, Jm, Jeu, Jem, Jms$	Post-Morrison	MF-152	Weir and others (1961)
33	Jn, Jel, Jeu, Je, Jem, Jmb, Kbc, Kd, Km	Post-Mancos; pre-Quaternary	MF-152	Weir and others (1961)
34	Jms, Jmb	Post-Morrison	I-360	Williams (1964)
35	Jem, Jms, Jmb	Post-Morrison	MF-152	Weir and others (1961)
36	Approximately located Km, Kms	Post-Mancos	MF-141	Weir and Puffett (1960)
37	Jmb, Kbc, Kd	Post-Dakota	MF-139	Carter and Gualtieri (1958)
38	Jw, Jk	Post-Kayenta	GQ-83	Shoemaker (1956b)
39	Jk, Jec	Post-Entrada and Carmel	GQ-71	Cater (1955b)
40	Jkw, Jse, Jmb	Post-Morrison	I-360	Williams (1964)
41	Jkw, Jse, Jmb	Post-Morrison	I-360	Williams (1964)
42	Jn, Jec, Js, Jms, Jmb, Kbc, Kd	Post-Dakota	MF-25	Cater (1955c)
43	Jmb, Kbc	Post-Burro Canyon	MF-203	Shawe and others (1961)
44	Pca, $\bar{K}mh, \bar{K}mu, \bar{K}m$	Post-Chinle	I-670	Hinrichs and others (1971)
45	Pcc, Pca, $\bar{K}mh, \bar{K}mu, \bar{K}cm, \bar{K}ecu, Jw, Jk, Jn$	Post-Navajo	I-670	Hinrichs and others (1971)
46	Pca, $\bar{K}mh, \bar{K}mu$	Post-Moenkopi	I-670	Hinrichs and others (1971)
47	Pcc, Pca	Post-Cutler	I-670	Hinrichs and others (1971)
48	Pca	Post-Cutler	I-670	Hinrichs and others (1971)

suggested by Witkind (1992), all three dominant fault sets of the Paradox basin (including the N. 45° E set trend) are younger than the uplift of the adjacent San Rafael Swell, all three sets must be somewhat younger than the Late Cretaceous or early Tertiary, possibly younger than Eocene and older than Pliocene. We note here that this age range cited by Witkind (p. 147) would encompass the 30–20-Ma ages of the La Sal Mountains and Henry Mountains laccolith complexes and is generally compatible with the post-Jurassic times of faulting shown in table 1. We reiterate that these faults, whose peak modal strike frequency is N. 45° E., fit the lineament correlation pattern described in previous sections of this report. The correlative lineaments probably represent faults or joints of similar ages.

This conclusion is based on the correspondence between azimuthal patterns of magnetic and gravity lineaments, presumably of Precambrian basement origin, and surface lineaments based on mapped faults, fold axes, and Landsat and radar lineaments (see Friedman and Heller, this volume). The azimuthal correspondence between structure at depth and lineaments and short extensional faults at the surface, as well as the predominantly Mesozoic and early

Tertiary times of faulting described above, suggests that many of the northeast-trending surface faults are of Mesozoic and Cenozoic age. Laramide compressive deformation of the craton caused by a clockwise rotation of about 2° or 4° of the Colorado Plateau region relative to the continental interior during Late Cretaceous and early Tertiary time (Hamilton, 1981) may have caused a reiteration of part of the Precambrian structural pattern in the near-surface geology, but with the intervening effect of salt solution and subsidence of overlying rock units along these predetermined directions.

Joint ages in Jurassic and Cretaceous rocks only, on the basis of field relations, are Laramide and post-Laramide. The older age of the northwest- and north-northwest-trending joints (fig. 10C) relative to the north-northeast- and northeast-trending joints (M.A. Grout, U.S. Geological Survey, written commun., 1991) also suggests a significant counterclockwise rotation of the stress field through time since the main phase of the Laramide orogeny, as documented for the adjacent Piceance Basin (Grout and Verbeek, 1991).

Although not included in the list of faults or lineaments of Quaternary age because of their semicircular or

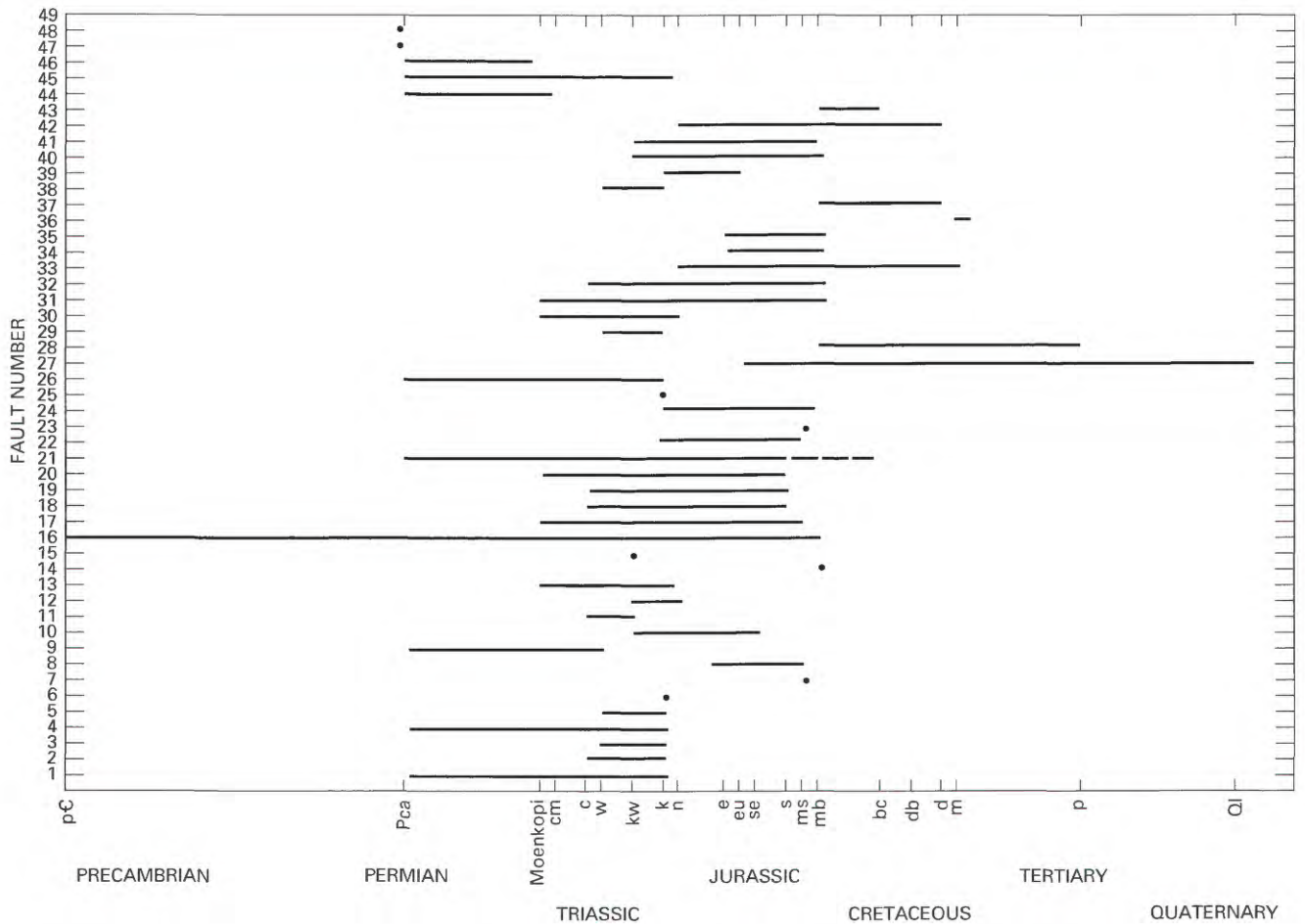


**Figure 18.** Diagram showing stratigraphic ages of formations cut by 48 northeast-striking faults in the Moab  $1^{\circ} \times 2^{\circ}$  quadrangle, northern Paradox Basin, Utah and Colorado. Each line shows time span represented by stratigraphic section cut by fault; most recent movement cannot be older than age represented by termination of line, which indicates youngest formation cut by fault. Dots indicate presence and age of overlying stratigraphic units that are not cut by fault; fault cannot be younger than overlying unit. Faults are located by number in figure 12 and listed with stratigraphic information in table 1.

semiconcentric character and diapiric (fig. 19) or solution-subsidence origin, the horst-graben terrain and bounding faults of the Needles fault zone are probably of Quaternary or even Holocene age (McGill and Stromquist, 1979; Huntoon, 1982).

## SUMMARY

1. Rose diagrams prepared uniformly from azimuthal histogram plots of several thousand lineaments of the Moab  $1^{\circ} \times 2^{\circ}$  quadrangle of southeastern Utah and southwestern Colorado permit statistical comparison of Landsat multispectral scanner lineament trends (and qualitative comparison of X-band radar lineament trends; see Friedman and Heller, this volume) with trends of magnetic- and gravity-field lineaments, surface joints, faults, and fold axes.

2. A good statistical correlation was found between major Landsat multispectral scanner lineaments, magnetic- and gravity-field lineaments, northwest-striking joints, fold axes, and northwest-trending faults. A similarly good correlation exists between the first-order surface azimuthal trends of all lineaments, length-weighted lineaments, and alignments mapped from Landsat multispectral scanner images and northeast-trending structural discontinuities in the Precambrian sequence as inferred from the magnetic field. The Precambrian structural discontinuities appear to be on a strike projection of the pre-Sinyala fault system of northern Arizona.

3. The good correspondence of azimuthal trends of magnetic- and gravity-field lineaments, presumably of Precambrian basement origin, and surface lineaments and mapped faults and joints suggests that structural reiterative patterns are likely to be present in the intervening



**Figure 19.** Aerial oblique view of Upheaval Dome and surrounding circular structure west of the Green River near Canyonlands, Utah. Deformed caprock units in fore- and middle-ground and deformed overlying beds have been cited as evidence of diapirism; however, more recently, listric fault structures, possible shatter cones, and other impact features suggested to E.M. Shoemaker (oral commun., 1992) an impact origin for Upheaval Dome. Photograph by Jules Friedman.

Phanerozoic sequence. Laramide and possible Pleistocene time of movement along the above-mentioned faults (mostly post-Early Jurassic time of faulting based on stratigraphic cutting relations) supports this conclusion. The surface lineaments and faults are thus interpreted to represent the reflection or reactivation of Precambrian basement-controlled structures in the younger Phanerozoic cover, partly through the intervening effect of salt solution and subsidence of overlying rock units along predetermined structural directions.

4. The major lineaments mapped (those longer than 20 km, 12.3 mi) show the best azimuthal correlation with lineaments of the magnetic field and mapped northwest-striking faults and fold axes and probably indirectly reflect deep faults in the Earth's crust. The location of the salt-cored anticlines is fault controlled northwest, as suggested by R.J. Hite (written commun., 1982) and others, but the thickness of their keels may be controlled by folds or grabens in the basement. The long and highly visible surface faulting associated with the salt-cored anticlines is principally the result of

solution and collapse of the salt, but the trends of the surface faulting give strong evidence of the trends of subsurface faults or folds that controlled emplacement and subsequent movement of the salt.

5. The laccolith complex of the La Sal Mountains and several circular features are at intersections of some of the major northwest- and northeast-trending lineaments of the Paradox Basin and are of special tectonic significance. The spacing of laccolith complexes, such as the La Sal, Abajo and others, and their possible occurrence at nodes of a northwest-northeast lineament grid suggest faulting down to the depth of the crust, where magmas are generated, and testifies to the deep-seated nature of the N. 40°–60° W. and N. 40°–50° E. discontinuities.

6. Circular features such as the Lockhart Basin and the semiconcentric Needles fault zone, below which salt solution and subsidence of the overlying sequence of clastic rocks have occurred, may represent the negative analog of salt diapirism in the Paradox Basin, and the generation of circular diapiric, intrusive, and subsidence structures may

indeed be related to the intersection of northeast-trending linear deep-seated faults, and northwest-trending faults or folds.

7. Surface faults such as fault clusters of an echelon character that lie astride the northeast-trending Precambrian structural discontinuities and concentric or circular features such as the Lockhart Basin and the semiconcentric Needles fault zone may have been significant in localizing halokinetic processes of salt flowage and dissolution. The Cenozoic and, indeed, Holocene development of the Needles fault zone may have occurred by gravity sliding and extensional structural displacement of the Phanerozoic sequence above the salt as the result of lubrication of the top of the salt by groundwater movement, in a process similar to that inferred by McGill and Stromquist (1979) and Huntoon (1982) and earlier workers.

8. Drainage pattern analysis suggests that the major northwesterly and northeasterly structural patterns and lineaments extend from the Uncompahgre Plateau at least as far southwest as Indian Creek, Harts Draw, Davis Canyon, Lavender Creek, and North Cottonwood Creek and the Needles fault zone.

## REFERENCES

- Affleck, J., and Hunt, C.B., 1980, Magnetic anomalies and structural geology of stocks and laccoliths in the Henry Mountains, Utah: Utah Geological Association, Henry Mountains Symposium, p. 107–112.
- Baars, D.L., and Stevinson, G.M., 1981, Tectonic evolution of the Paradox Basin, Utah and Colorado, in Wiegand, D.E., ed., Guidebook to the geology of the Paradox Basin: Rocky Mountain Association of Geologists Field Conference, p. 23–31.
- Badgley, P.C., 1962, Analysis of structural patterns in bedrock: American Institute Mining, Metallurgy, Petroleum Engineers, Society Mining Engineers Transactions, v. 225, no. 12, p. 381–389.
- Bloom, A.L., 1978, Geomorphology—A systematic analysis of late Cenozoic landforms: Englewood Cliffs, N.J., Prentice-Hall, 510 p.
- Carter, W.D., and Gualtieri, J.L., 1958, Preliminary geologic map of the Mount Peale 1° NW quadrangle, San Juan County, Utah: U.S. Geological Survey Mineral Investigations Field Studies Map MF-140, scale 1:24,000.
- Carter, W.D., Gualtieri, J.L., and Shoemaker, E.M., 1958, Preliminary geologic map of the Mount Peale 1° NE quadrangle, San Juan County, Utah, and Montrose County, Colorado: U.S. Geological Survey Mineral Investigations Field Studies Map MF-139, scale 1:24,000.
- Case, J.E., 1991, Geologic map of the northwestern part of the Uncompahgre uplift, Grand County, Utah and Mesa County, Colorado, with emphasis on Proterozoic rocks: U.S. Geological Survey Miscellaneous Investigations Series Map I-2088, scale 1:24,000.
- Case, J.E., and Joesting, H.R., 1973, Regional geophysical investigations on the central Colorado Plateau: U.S. Geological Survey Professional Paper 736, 31 p.
- Case, J.E., Joesting, H.R., and Byerly, P.C., 1963, Regional geophysical investigations in the La Sal Mountains area, Utah and Colorado: U.S. Geological Survey Professional Paper 316-F, p. 91–116.
- Cashion, W.B., compiler, 1973, Geologic and structure map of the Grand Junction quadrangle, Colorado-Utah: U.S. Geological Survey Miscellaneous Investigations Map I-736, scale 1:250,000.
- Cashion, W.B., Kilburn, J.E., Barton, H.N., Kelley, K.D., Kulik, D.M., and McDonnell, J.R., Jr., 1990, Mineral resources of the Desolation Canyon, Turtle Canyon, and Floy Canyon Wilderness Study Areas, Carbon, Emery, and Grand Counties, Utah: U.S. Geological Survey Bulletin 1753, p. B18.
- Cater, F.W., Jr., 1955a, Geology of the Pine Mountain quadrangle, Colorado: U.S. Geological Survey Geologic Quadrangle Map GQ-60, scale 1:24,000.
- 1955b, Geology of the Davis Mesa quadrangle: U.S. Geological Survey Quadrangle Map GQ-71, scale 1:24,000.
- 1955c, Preliminary geologic map of the Anderson Mesa quadrangle, Colorado: U.S. Geological Survey Mineral Investigations Field Studies Map MF-25, scale 1:24,000.
- Dane, C.H., 1931, Uncompahgre Plateau and related structural features [abs.]: Washington Academy of Sciences Journal, v. 21, no. 2, p. 28.
- 1935, Geology of the Salt Valley anticline and adjacent areas, Grand County, Utah: U.S. Geological Survey Bulletin 863, 184 p.
- Doelling, H.H., 1985, Geology of Arches National Park: Utah Geological and Mineral Survey Map 74, 15 p.
- Dubiel, R.F., 1989, Sedimentology and revised nomenclature for the upper part of the Upper Triassic Chinle Formation and Lower Jurassic Wingate Sandstone, northwestern New Mexico and northeastern Arizona: New Mexico Geological Society Annual Field Conference, 40th, Guidebook, p. 213–223.
- Eardley, A.J., 1951, Structural geology of North America: New York, Harper and Brothers, 624 p.
- Ekren, E.B., and Houser, F.N., 1965, Geology and petrology of the Ute Mountains area, Colorado: U.S. Geological Survey Professional Paper 481, 74 p.
- Elston, D.P., and Shoemaker, E.M., 1961, Preliminary structure contour map on top of salt in the Paradox Formation of the Hermosa Formation in the salt anticline region, Colorado and Utah: U.S. Geological Survey Oil and Gas Investigations Map OM-209, scale 1:250,000.
- Fitterman, D.V., 1982, Magnetometric resistivity survey near Hatch Point and Lockhart Basin, San Juan County, Utah: U.S. Geological Survey Open-File Report 82-400, 52 p.
- Frahme, C.W., 1984, Paleozoic geology and seismic stratigraphy of the northern Uncompahgre front, Grand County, Utah: Earth Science Bulletin of the Wyoming Geological Association, v. 17, p. 101.
- Frahme, C.W., and Vaughn, E.B., 1983, Paleozoic geology and seismic stratigraphy of the northern Uncompahgre front, Grand County, Utah: Rocky Mountain Association of Geologists, p. 201–211.
- Friedman, J.D., and Simpson, S.L., 1978, Landsat investigations of the northern Paradox Basin, Utah and Colorado—Implications for radioactive waste emplacement; Part 1, Lineaments and alignments: U.S. Geological Survey Open-File Report 78-900, 49 p.

- 1980, Lineaments and geologic structure of the northern Paradox Basin, Colorado and Utah: U.S. Geological Survey Miscellaneous Field Studies Map MF-1221, scale 1:500,000.
- Frost, R.T.C., 1977, Tectonic patterns in the Danish region (as deduced from a comparative analysis of magnetic, Landsat, bathymetric and gravity lineaments): *Geologie en Mijnbouw*, v. 56, no. 4, p. 351-362.
- Grout, M.A., and Verbeek, E.R., 1991, Fracture history of the Divide Creek and Wolf Creek anticlines and its relation to Laramide Basin-margin tectonism, southern Piceance Basin, northwestern Colorado: U.S. Geological Survey Bulletin 1787-Z, 32 p.
- Hackman, R.J., 1959a, Photogeologic map of the Coach Creek NE quadrangle, Grand County, Utah, and Mesa County, Colorado: U.S. Geological Survey Miscellaneous Investigations Map I-279, scale 1:24,000.
- 1959b, Photogeologic map of the Coach Creek SE quadrangle, Grand County, Utah, and Mesa County, Colorado: U.S. Geological Survey Miscellaneous Investigations Map I-278, scale 1:24,000.
- Hamblin, W.K., 1970, Structure of the western Grand Canyon region: Utah Geological Society Guidebook 23, p. 3-19.
- Hamilton, W.B., 1981, Plate-tectonic mechanism of Laramide deformation: University of Wyoming Contributions to Geology, v. 19, p. 87-92.
- 1989, Crustal geologic processes of the United States, *in* Pakiser, L.C., and Mooney, W.D., eds., Geophysical framework of the continental United States: Geological Society of America Memoir 172, p. 743-781.
- Hansen, W.R., 1981, Geologic and physiographic highlights of the Black Canyon of the Gunnison River and vicinity, Colorado, *in* Epis, R.C., and Callender, J.F., eds., Western Slope Colorado: New Mexico Geological Society Annual Field Conference, 32nd, October 8-10, 1981, Guidebook, p. 145-154.
- Hayden, F.V., 1877, Geological and geophysical atlas of Colorado and portions of adjacent territory: U.S. Geological and Geographical Surveys, Sheet 17.
- Hildenbrand, T.G., and Kucks, R.P., 1983, Regional magnetic and gravity features of the Gibson Dome area and surrounding region, Paradox Basin, Utah—A preliminary report: U.S. Geological Survey Open-File Report 83-359, 34 p.
- Hinrichs, E.N., Krummel, W.J., Jr., Connor, J.J., and Moore, H.J., 3rd, 1971, Geologic map of the southwest quarter of the Hatch Point Quadrangle, San Juan County, Utah: U.S. Geological Survey Miscellaneous Investigations Map I-670, scale 1:24,000.
- Hinrichs, E.N., Krummel, W.J., Jr., Moore, H.J., 3rd, and Conner, J.J., 1968, Geologic map of the northeast quarter of the Hatch Point quadrangle, San Juan County, Utah: U.S. Geological Survey Miscellaneous Investigations Map I-526, scale 1:24,000.
- Hite, R.J., 1961, Potash-bearing evaporite cycles in the salt anticlines of the Paradox Basin, Colorado and Utah, *in* Short papers in the geologic and hydrologic sciences: U.S. Geological Survey Professional Paper 424-D, p. D135-138.
- 1975, An unusual northeast-trending fracture zone and its relation to basement wrench faulting in northern Paradox Basin, Utah and Colorado, *in* Canyonlands: Four Corners Geological Society Field Conference, 8th, Canyonlands Country, Guidebook, p. 217-224.
- Hite, R.J., and Lohman, S.W., 1973, Geologic appraisal of Paradox Basin and salt deposits for waste emplacement: U.S. Geological Survey Open-File Report, 75 p.
- Hobbs, W.H., 1904, Lineaments of the Atlantic border region: Geological Society of America Bulletin, v. 15, p. 483-506.
- 1912, Earth features and their meaning: New York, Macmillan, 506 p.
- Holmes, C.N., 1956, Tectonic history of the ancestral Uncompahgre Range in Colorado, *in* Geology and economic deposits of east central Utah: Intermountain Association of Petroleum Geologists Annual Field Conference, 7th, Guidebook, p. 190-194.
- Howard, A.D., 1967, Drainage analysis in geologic interpretation—A summation: American Association of Petroleum Geologists Bulletin, v. 51, p. 2246-59.
- Howard, K.A., Aaron, J.M., Brabb, E.E., Brock, M.R., Gower, H.D., Hunt, S.J., Milton, D.J., Muehlberger, W.R., Nakata, J.K., Plafker, G., Prowell, D.C., Wallace, R.E., and Witkind, I.J., 1978, Preliminary map of young faults in the United States as a guide to possible fault activity: U.S. Geological Survey Mineral Investigations Field Studies Map MF-916, scales 1:5,000,000, 1:7,500,000.
- Hunt, C.B., and Waters, A.C., 1958, Structural and igneous geology of the La Sal Mountains: U.S. Geological Survey Professional Paper 2941-I, p. 305-364.
- Hunt, G.L., 1988, Petrology of the Mt. Pennell central stock, Henry Mountains, Utah: Brigham Young University Geology Studies, v. 35, p. 81-100.
- Huntoon, P.W., 1982, The Meander anticline, Canyonlands, Utah—An unloading structure resulting from horizontal gliding on salt: Geological Society of America Bulletin, v. 93, no. 10, p. 941-950.
- Huntoon, P.W., and Richter, H.R., 1979, Breccia pipes in the vicinity of Lockhart Basin, Canyonlands area, Utah: Four Corners Geological Society Field Conference, 9th, Guidebook, p. 47-53.
- Jackson, M.D., and Pollard, D.D., 1988, The laccolith-stock controversy—New results from the southern Henry Mountains, Utah: Geological Society of America Bulletin, v. 100, p. 117-139.
- Johnson, V.C., 1983, Preliminary aeromagnetic interpretation of the Uncompahgre uplift and Paradox Basin, west-central Colorado and east-central Utah; Grand Junction Geological Society, 1983 Field Trip, Proceedings, p. 67-70.
- Kelley, V.C., 1956, Influence of regional structure and tectonic history upon the origin and distribution of uranium on the Colorado plateau: U.S. Geological Survey Professional Paper 300, p. 171-178.
- Khazov, R.A., 1980, Metallogenic belt of long-evolving deep faults in the southeast fringe of the Baltic shield: *Doklady Akademii Nauk SSSR*, v. 255, no. 4, p. 949-953.
- Kosygin, Yu.A., Yushmanov, V.V., Maslov, L.A., 1980, Generation of concentric complexes (ring structures) by development of linear faults [trans.]: *Doklady Akademii Nauk SSSR*, v. 255, no. 6, p. 1454-1458.
- Maarouf, Abdelrahman, 1983, Relationship between basement faults and Colorado Plateau drainage: Grand Junction Geological Society 1983 Field Trip, Northern Paradox Basin—Uncompahgre Uplift, Guidebook, p. 59-62.
- McGill, G.E., and Stromquist, A.W., 1979, The grabens of Canyonlands National Park, Utah—Geometry, mechanics, and

- kinematics: *Journal of Geophysical Research*, v. 84, no. B9, p. 4547–4563.
- Mutschler, F.E., and Hite, R.J., 1969, Origin of the Meander anticline, Cataract Canyon, Utah, and basement control of Colorado River drainage: *Geological Society of America Abstracts with Programs for 1969*, pt. 5, p. 57–58.
- Nelson, S.T., Heizler, M.J., and Davidson, J.P., 1992, New  $^{40}\text{Ar}/^{39}\text{Ar}$  ages of intrusive rocks from the Henry and La Sal Mountains, Utah: *Utah Geological Survey Miscellaneous Publication 92-2*, 23 p.
- Nelson, S.T., Sullivan, K.R., and Davidson, J.P., 1992, New age determinations of central Colorado Plateau laccoliths, Utah—Recognizing disturbed K-Ar systematics and re-evaluating tectonomagmatic relationships: *Geological Society of America Bulletin*, v. 104, p. 1547–1560.
- O'Leary, D.W., Friedman, J.D., and Pohn, H.A., 1976, Lineament, linear, lineation—Some proposed new standards for old terms: *Geological Society of America Bulletin*, v. 87, p. 1463–1469.
- Plescia, J.B., and Henyey, T.L., 1982, Geophysical character of the proposed eastern extension of the Garlock fault and adjacent areas, eastern California: *Geology*, v. 10, no. 4, p. 209–214.
- Sawatzky, D.L., and Raines, G.L., 1981, Geologic uses of linear feature maps from small-scale images, *in* O'Leary, D.W., and Earle, J.L., eds., *International Conference New Basement Tectonics*, 3rd, Proceedings; *Basement Tectonics Committee, Publication 3*, p. 91–100.
- Shaw, D.R., Simmons, G.C., and Rogers, W.B., 1961, Preliminary geologic map of the Slick Rock district, San Miguel and Dolores Counties, Colorado: *U.S. Geological Survey Mineral Investigations Field Studies Map MF-203*, scale 1:48,000.
- Shaw, H.R., 1980, The fracture mechanism of magma transport from the mantle to the surface, *in* Hargraves, R.B., ed., *Physics of magmatic processes*: Princeton, N.J., Princeton University Press, p. 201–264.
- Shoemaker, E.M., 1955, Geology of the Juanita Arch quadrangle: *U.S. Geological Survey Geologic Quadrangle Map GQ-81*, scale 1:24,000.
- , 1956a, Structural features of the central Colorado Plateau and their relationship to uranium deposits: *U.S. Geological Survey Professional Paper 300*, p. 155–170.
- , 1956b, Geology of the Rock Creek quadrangle: *U.S. Geological Survey Geologic Quadrangle Map GQ-83*, scale 1:24,000.
- Shoemaker, E.M., Squires, R.L., and Abrams, M.J., 1978, Bright Angel and Mesa Butte fault systems of northern Arizona, *in* Smith, R.B., and Eaton, G.P., eds., 1978, *Cenozoic tectonics and regional geophysics of the Western Cordillera*: *Geological Society of America Memoir 152*, p. 341–367.
- Sloss, L.L., 1988, Tectonic evolution of the craton in Phanerozoic time, *in* Sloss, L.L., ed., *Sedimentary cover—North American craton*: *Geological Society of America, The Geology of North America*, v. D-2, p. 25–37.
- Stern, T.W., Newell, M.F., Kistler, R.W., and Shawe, D.R., 1965, Zircon uranium-lead and thorium-lead ages and mineral potassium-argon ages of La Sal Mountains rocks, Utah: *Journal of Geophysical Research*, v. 70, no. 6, p. 1504–1507.
- Stevinson, G.M., and Baars, D.L., 1986, The Paradox pull-apart basin, Pennsylvanian rejuvenation of basement lineaments [abs.]: 5th, *International Conference on Basement Tectonics, Proceedings*, p. 310.
- Stokes, W.L., 1948, Geology of the Utah Colorado salt dome region, with emphasis on Gypsum Valley, Colorado: *Utah Geological Society Guidebook 3*, p. 50.
- , 1986, *Geology of Utah*: Utah Museum of Natural History and Utah Geological and Mineral Survey, p. 233–234.
- Stone, D.S., 1977, Tectonic history of the Uncompahgre uplift, *in* *Exploration frontiers of the central and southern Rockies*: *Rocky Mountain Association of Geologists Guidebook*, p. 23–30.
- Sullivan, K.R., Kowallis, B.J., and Mehnert, H.W., 1991, Isotopic ages of igneous intrusions in southeastern Utah—Evidence for a mid-Cenozoic Reno-San Juan magmatic zone: *Brigham Young University Geology Studies*, v. 37, p. 139–144.
- Sutphin, H.A., and Wenrich, K.J., 1988, Map showing structural control at breccia pipes on the southern Marble Plateau, north-central Arizona: *U.S. Geological Survey Miscellaneous Investigations Series Map I-1778*, scale 1: 50,000.
- Szabo, Ernest, and Wengert, S.A., 1975, Stratigraphy and tectogenesis of the Paradox Basin: *Four Corners Geological Society Field Conference*, 8th, *Canyonlands Country, Guidebook*, p. 193–210.
- Tolbert, G.E., 1956, Photogeologic map of the Carlisle-1 quadrangle, San Juan County, Utah: *U.S. Geological Survey Miscellaneous Investigations Map I-180*, scale 1:24,000.
- Tweto, Ogden, 1980, Tectonic history of Colorado, *in* Kent, H.S., and Porter, K.W., eds., *Colorado geology*: *Rocky Mountain Association of Geologists Guidebook*, p. 5–9.
- Warner, L.A., 1978, The Colorado lineament—A middle Precambrian wrench fault system: *Geological Society of America Bulletin*, v. 89, no. 2, p. 161–171.
- Watts, R.D., 1982, Interpretation of Schlumberger DC resistivity data from Gibson dome-Lockhart basin study area, San Juan County, Utah: *U.S. Geological Survey Open-File Report 82-0704*, 21 p.
- Weir, G.W., Kennedy, V.C., Puffett, W.P., and Dodson, C.L., 1961, Preliminary geologic map and section of the Mount Peale 2° NW quadrangle, San Juan County, Utah: *U.S. Geological Survey Mineral Investigations Field Studies Map MF-152*, scale 1:24,000.
- Weir, G.W., and Puffett, W.P., 1960, Preliminary geologic map and sections of the Mount Peale 2° NE quadrangle, San Juan County, Utah: *U.S. Geological Survey Mineral Investigations Field Studies Map MF-141*.
- Williams, P.L., 1964, Geology, structure, and uranium deposits of the Moab quadrangle, Colorado and Utah: *U.S. Geological Survey Miscellaneous Geologic Investigations Map I-360*, scale 1:250,000.
- Witkind, I.J., 1975, The Abajo Mountains—An example of the laccolithic groups on the Colorado Plateau: *Four Corners Geological Society Field Conference*, 8th, *Canyonlands Country, Guidebook*, p. 245–252.
- , 1992, Implications of distinctive fault sets in the San Rafael Swell and adjacent areas, east-central Utah: *Utah Geological Association Publication 19*, p. 141–148.
- Wong, I.G., Humphrey, J.R., Kollmann, A.C., Munden, B.B., and Wright, D.D., 1987, Earthquake activity in and around Canyonlands National Park, Utah: *Four Corners Geological Society Field Conference*, 10th, *Cataract Canyon, Guidebook*, p. 51–58.
- Yegorov, Yu.I., 1981, Distribution and classification of faults in the southern part of the Siberian platform: *Doklady Akademii Nauk SSSR*, v. 257, no. 3, p. 687–690.
- Zoback, M.L., and Zoback, M.D., 1989, Tectonic stress field of the continental United States, *in* Pakiser, L.C., and Mooney, W.D., *Geophysical framework of the continental United States*: *Geological Society of America Memoir 172*, p. 523–539.

# Uncontrolled X-Band Radar Mosaic of the Western Part of the Moab 1°×2° Quadrangle, Southeastern Utah and Southwestern Colorado

By Jules D. Friedman *and* Joan S. Heller

EVOLUTION OF SEDIMENTARY BASINS—PARADOX BASIN

A.C. Huffman, Jr., Project Coordinator

---

U.S. GEOLOGICAL SURVEY BULLETIN 2000–D

*A multidisciplinary approach to research studies of  
sedimentary rocks and their constituents and  
the evolution of sedimentary basins, both ancient and modern*



UNITED STATES GOVERNMENT PRINTING OFFICE, WASHINGTON : 1994



# CONTENTS

Abstract.....	D1
Introduction.....	1
Image Geometry .....	1
Slant-Range Scale Distortion.....	5
Tectonic Interpretation of Selected Radar Images.....	8
References Cited.....	10

## PLATE

[Plate is in pocket]

1. Uncontrolled X-band radar mosaic of the western part of the Moab 1°×2° quadrangle, southeastern Utah and southwestern Colorado.

## FIGURES

1. Diagram showing geometry of X-band slant-range radar images in relation to hypothetical ground-range presentation.....	D2
2. Graph showing depression angles to the two edges of slant-range radar images of the Moab 1°×2° quadrangle.....	2
3, 4. Diagrams showing:	
3. Extent of slant-range radar image coverage of the Moab 1°×2° quadrangle .....	2
4. Geometry of the sidelap coverage of slant-range radar images of the Moab 1°×2° quadrangle.....	2
5-9. X-band radar images and geologic maps:	
5. Polar Mesa area .....	3
6. Colorado River valley between Dry Gulch fault zone and Fisher Valley.....	4
7. Region between Spanish Valley at Moab and Indian Point.....	6
8. Needles fault zone, Canyonlands .....	8
9. Green River area between Salt Wash and Cottonwood grabens .....	9



# Uncontrolled X-Band Radar Mosaic of the Western Part of the Moab 1°×2° Quadrangle, Southeastern Utah and Southwestern Colorado

By Jules D. Friedman *and* Joan S. Heller

## ABSTRACT

An uncontrolled X-band airborne radar-image mosaic was compiled for the western three-fifths of the Moab 1°×2° quadrangle, southeastern Utah and southwestern Colorado, to assess surface fractures (including joints) that might provide evidence for tectonic trends at depth.

Five areas within the mosaic were selected for their depiction of topographic and structural detail. The approximate strike of linear features observed on the radar images can be inferred by comparison with rectified Landsat multispectral scanner images and geologic maps.

The radar images display a strong N. 37°–65° E. trend representing joint sets and extensional fractures that have little or no offset, as well as extensional high-angle faults of the same trend, of generally Laramide or post-Laramide age, that have predominantly vertical offset. The radar images also clearly depict examples, such as the Moab fault system, of the first-order (most common) fault trend in this part of the Paradox Basin, a trend that coincides in large part with the first-order gravity (N. 40°–60° W.) and magnetic (N. 40°–60° W.) field trends and is generally parallel to the fold axes of the major salt anticlines of the Paradox Basin and the southwestern thrust fault zone bounding the Uncompahgre uplift.

## INTRODUCTION

The objective of the Paradox Basin remote-sensing project of the U.S. Geological Survey is to acquire, process, and interpret geologically a variety of satellite and aircraft image products of the region in order to assess factors in the tectonic and geomorphic environment that may provide clues to deep-seated tectonic trends. In line with this objective, a radar mission was flown over the Paradox Basin (western part of the Moab 1°×2° quadrangle, lat 38°–39° N.,

long 109°–110° W.) for the U.S. Geological Survey, October 23, 1979, by a Convair 580 aircraft of the Canada Center for Remote Sensing; the aircraft was equipped with Environmental Research Institute of Michigan (ERIM) XL-band radar. High-quality slant-range radar images were obtained, including coverage of the Salt Valley, Gibson Dome, and Lisbon Valley areas, for geomorphic and structural investigations. A small part of the adjoining Salina 1°×2° quadrangle was included in the survey and is discussed later.

This report is a companion to Friedman and others (this volume), a discussion of tectonic trends of the northern Paradox Basin as derived from Landsat multispectral scanner images and geophysical and geologic maps.

*Acknowledgments.*—Allan N. Kover and Marilyn A. Grout kindly reviewed the manuscript.

## IMAGE GEOMETRY

A description of the geometry of X-band slant-range radar images of the Moab quadrangle is shown in figure 1. Each line imaged was divided into two subswaths because two cathode-ray tube recorders were used to record wide-swath data. Six flight lines were flown over the region; 12 subswaths of data were produced. The data were collected at an aircraft altitude of 17,000 ft (5,182 m) above sea level. The distance from the aircraft to the near edge of the image is 13,000 ft (3,962 m). The depression angle to the proximal edge of the image ( $\theta_n$ ) is

$$\theta_n = \arcsin \frac{17,000 - E}{13,000}, \quad (1)$$

where  $E$  is the terrain elevation in feet above sea level. For a terrain elevation of 6,000 ft (1,829 m), the depression angle to the proximal edge ( $\theta_n$ ) is 57.8°.

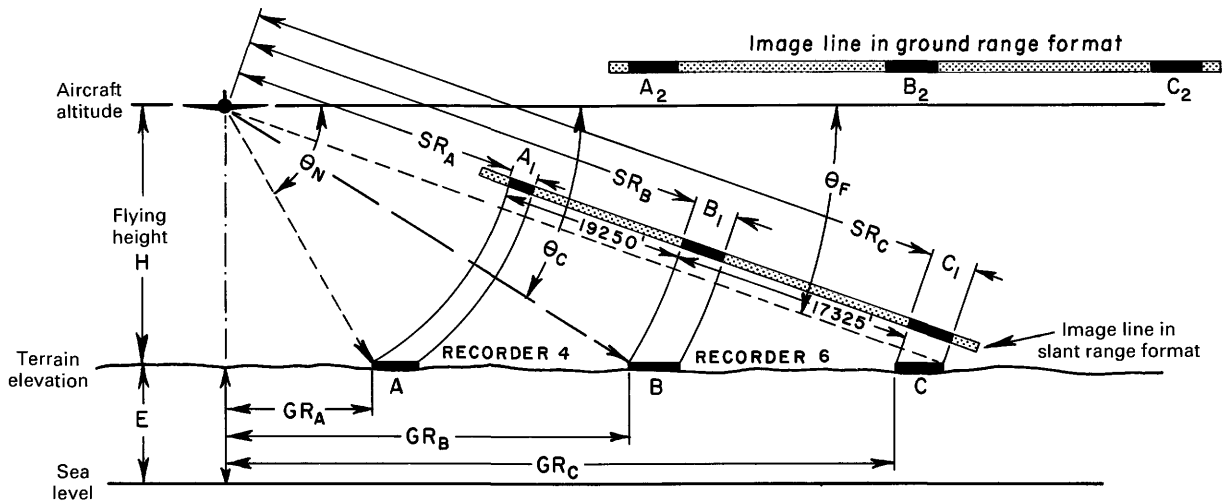


**Figure 1.** Geometry of X-band slant-range radar images in relation to a hypothetical ground-range presentation.

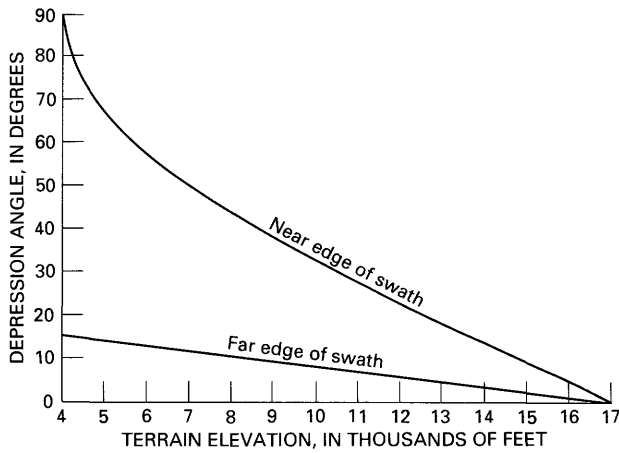


**Figure 2.** Depression angles to the two edges of slant-range radar images of the Moab 1°x2° quadrangle, southeastern Utah and southwestern Colorado.

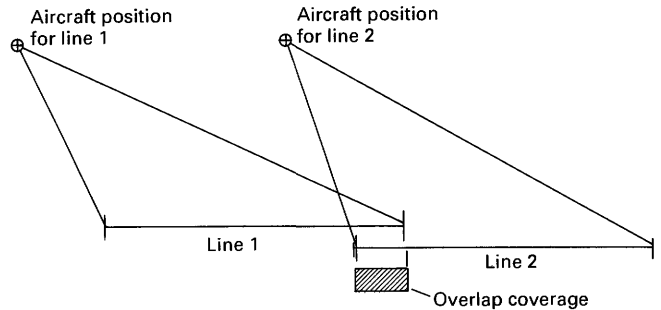


**Figure 4.** Geometry of the sidelap coverage of slant-range radar images of the Moab 1°x2° quadrangle, southeastern Utah and southwestern Colorado.

The depression angle to the center of the swath ( $\theta_c$ ) is

$$\theta_c = \arcsin \frac{17,000 - E}{32,250}, \quad (2)$$

and the depression angle to the distal edge ( $\theta_f$ ) is

$$\theta_f = \arcsin \frac{17,000 - E}{49,575}. \quad (3)$$

Again, for  $E$  equal to 6,000 ft (1,829 m),  $\theta_c=19.9^\circ$  and  $\theta_f=12.8^\circ$ . The ground range ( $GR_A$ ) from the aircraft ground track to the proximal edge of the image is

$$GR_A = 13,000 \cos \arcsin \frac{17,000 - E}{13,000}, \quad (4)$$

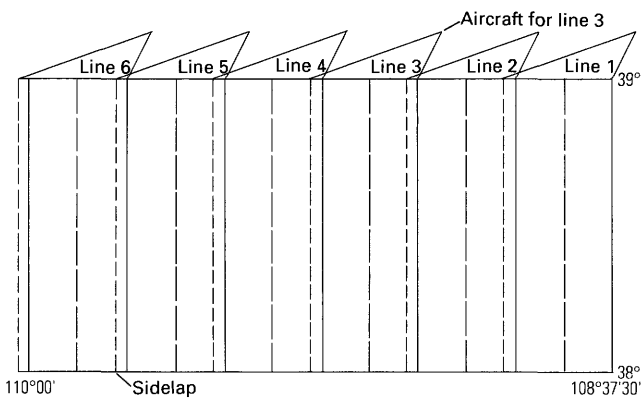


**Figure 3.** Extent of slant-range radar image coverage of the Moab 1°x2° quadrangle, southeastern Utah and southwestern Colorado.

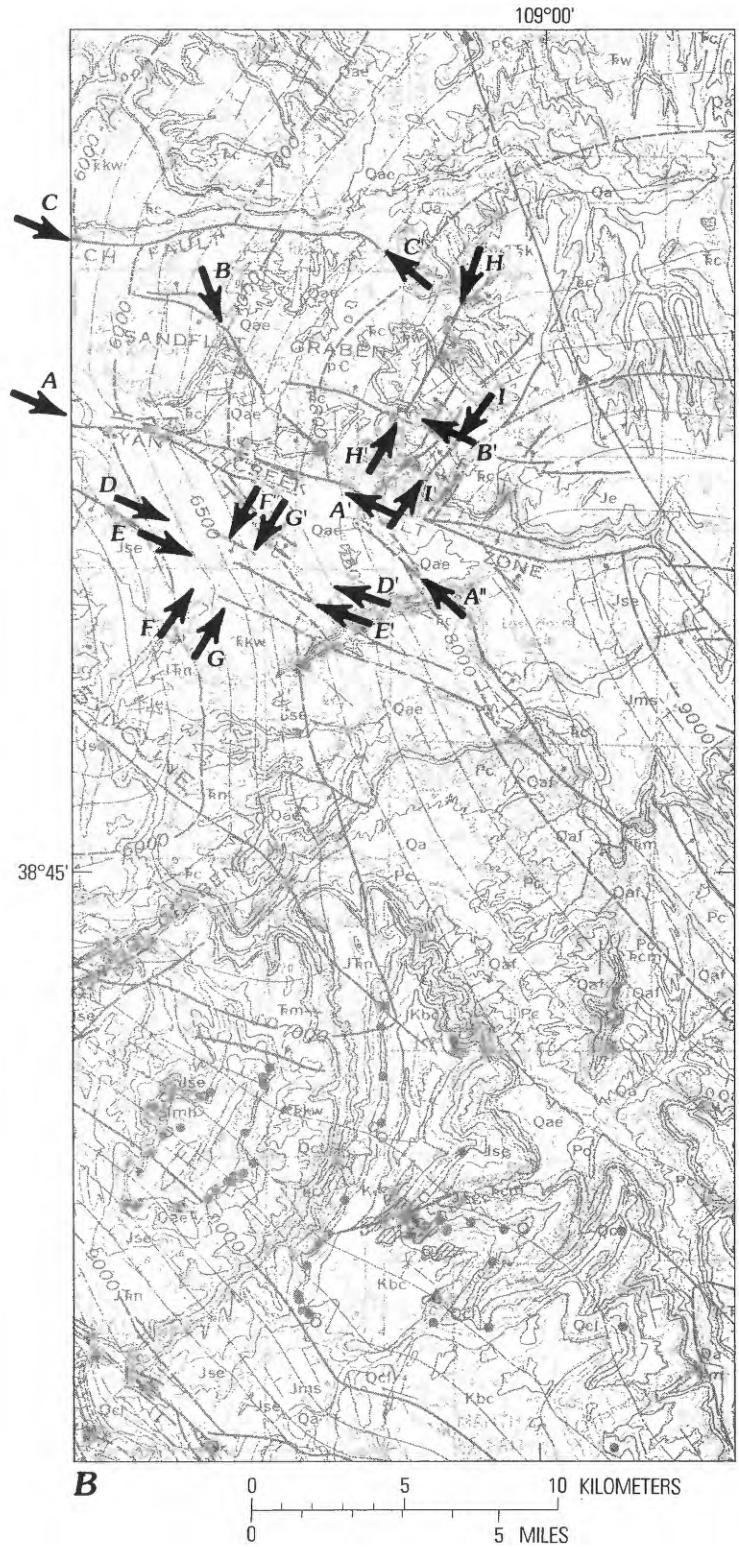
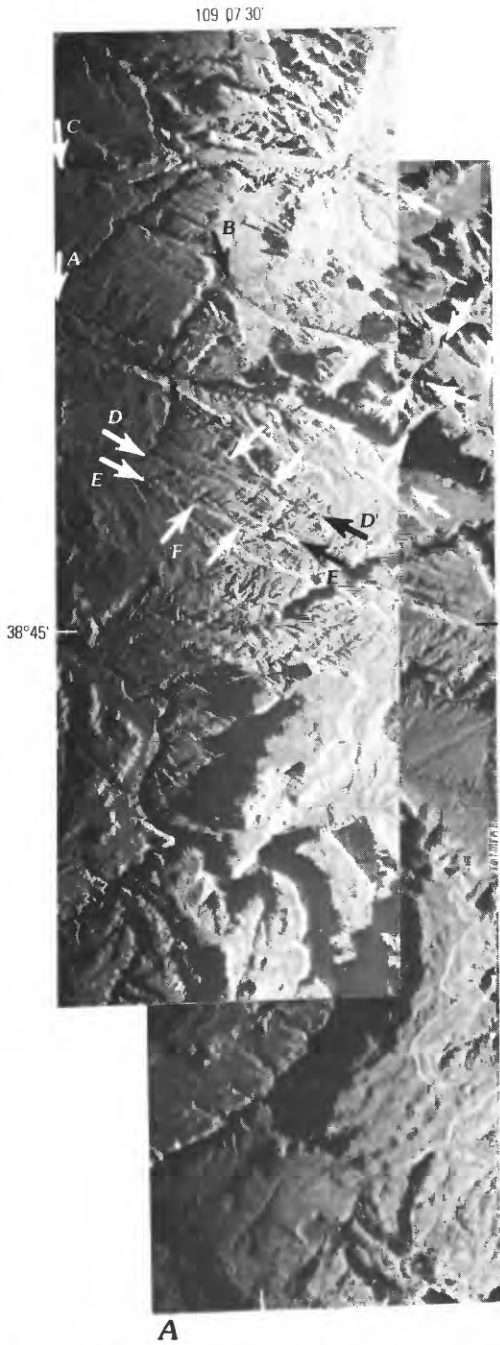


**Figure 5.** Polar Mesa area, Utah and Colorado. *A-A'-A''*, Ryan Creek fault zone. *B-B'*, faults of Sand Flat graben. *C-C'*, Dry Gulch fault zone. *D-D'* and *E-E'*, northwest-striking faults and lineaments. *F-F'* and *G-G'*, previously unmapped northeast-trending fracture system reflected in topography; movement along fractures probably is mostly extension. *H-H'* and *I-I'*, geologically mapped northeast-trending faults cutting both Precambrian and Jurassic sequences. *A*, X-band radar image. *B*, Geologic structure. Modified from Williams (1964).

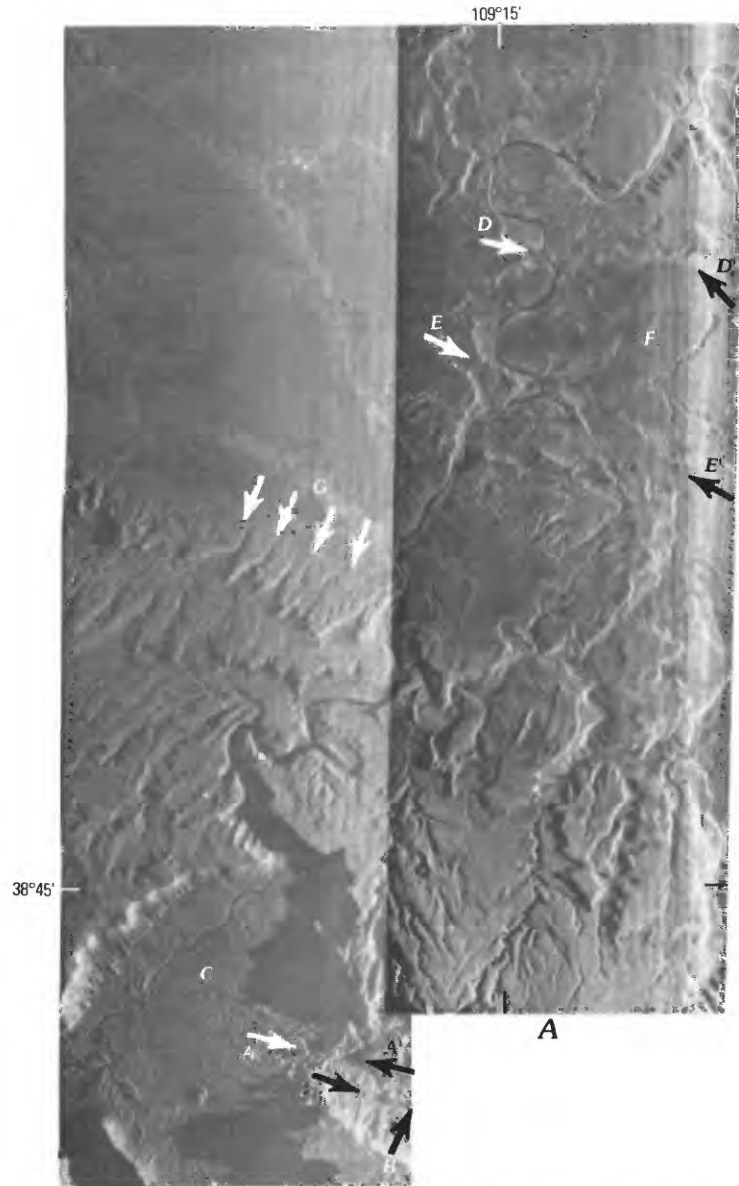


**Figure 6 (above and facing page).** Colorado River valley between Dry Gulch fault zone and Fisher Valley. *A-A'* and *B-B'*, segments of bounding faults along crest of Fisher Valley anticline. *C*, Richardson Amphitheater (Cutler Formation of Early Permian age). North boundary fault (Dry Gulch fault zone) (*D-D'*) and south boundary fault (Ryan Creek fault zone) (*E-E'*) of *F*, Sand Flat graben. *G*, arroyo development on northeast-trending joints on southwest flank of Sagers Wash syncline. *A*, X-band radar image. *B*, Geologic structure. Modified from Williams (1964).

for the center of the swath ( $GR_B$ )

$$GR_B = 32,250 \cos \arcsin \frac{17,000 - E}{32,250}, \quad (5)$$

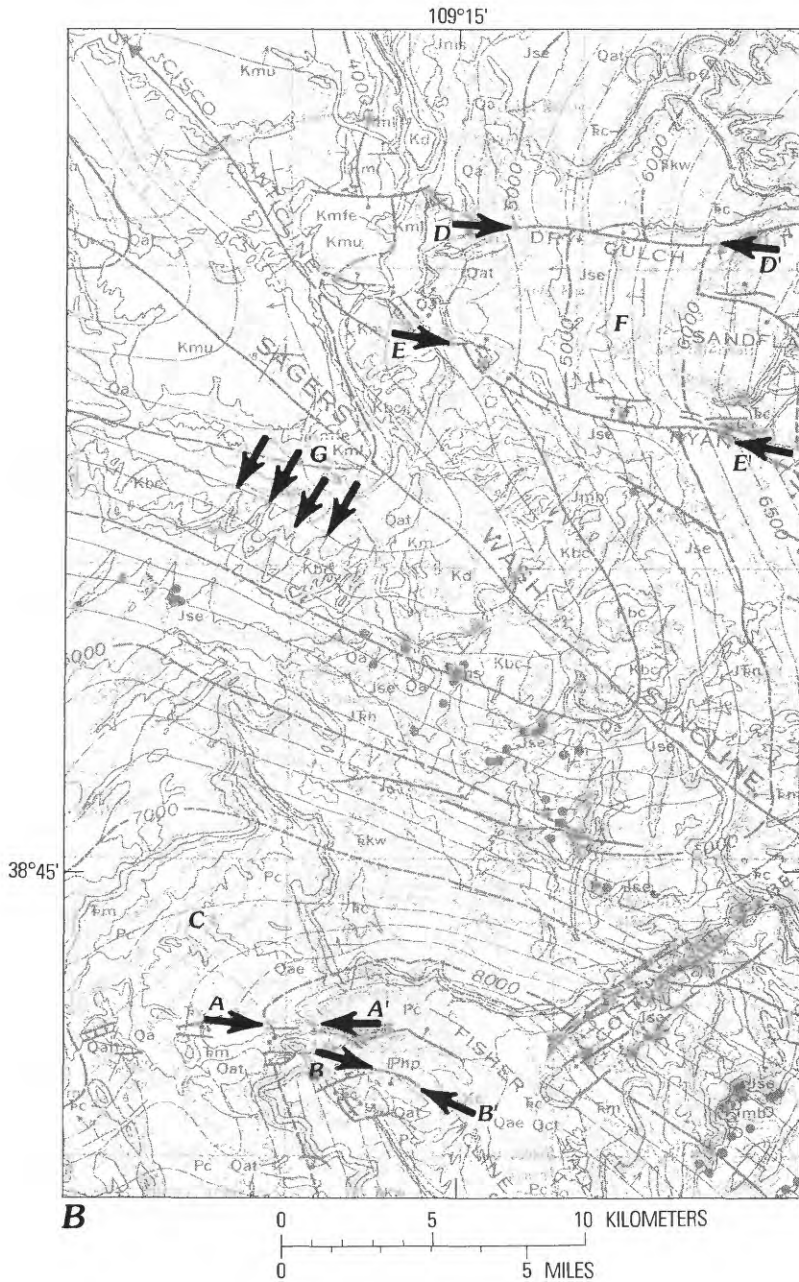
and to the distal edge ( $GR_C$ )

$$GR_C = 42,575 \cos \arcsin \frac{17,000 - E}{49,575}, \quad (6)$$

Using the example of  $E=6,000$  ft (1,829 m), then

$$\begin{aligned} GR_A &= 6,927 \text{ ft (2,111 m),} \\ GR_B &= 30,234 \text{ ft (9,215 m), and} \\ GR_C &= 48,343 \text{ ft (14,735 m).} \end{aligned}$$

The ground swath width is  $GR_C - GR_A$  and is 41,416 ft (12,625 m) for  $E=6,000$  ft (1,829 m). The depression angles to the two edges of the image are shown in figure 2 as a function of terrain elevation.

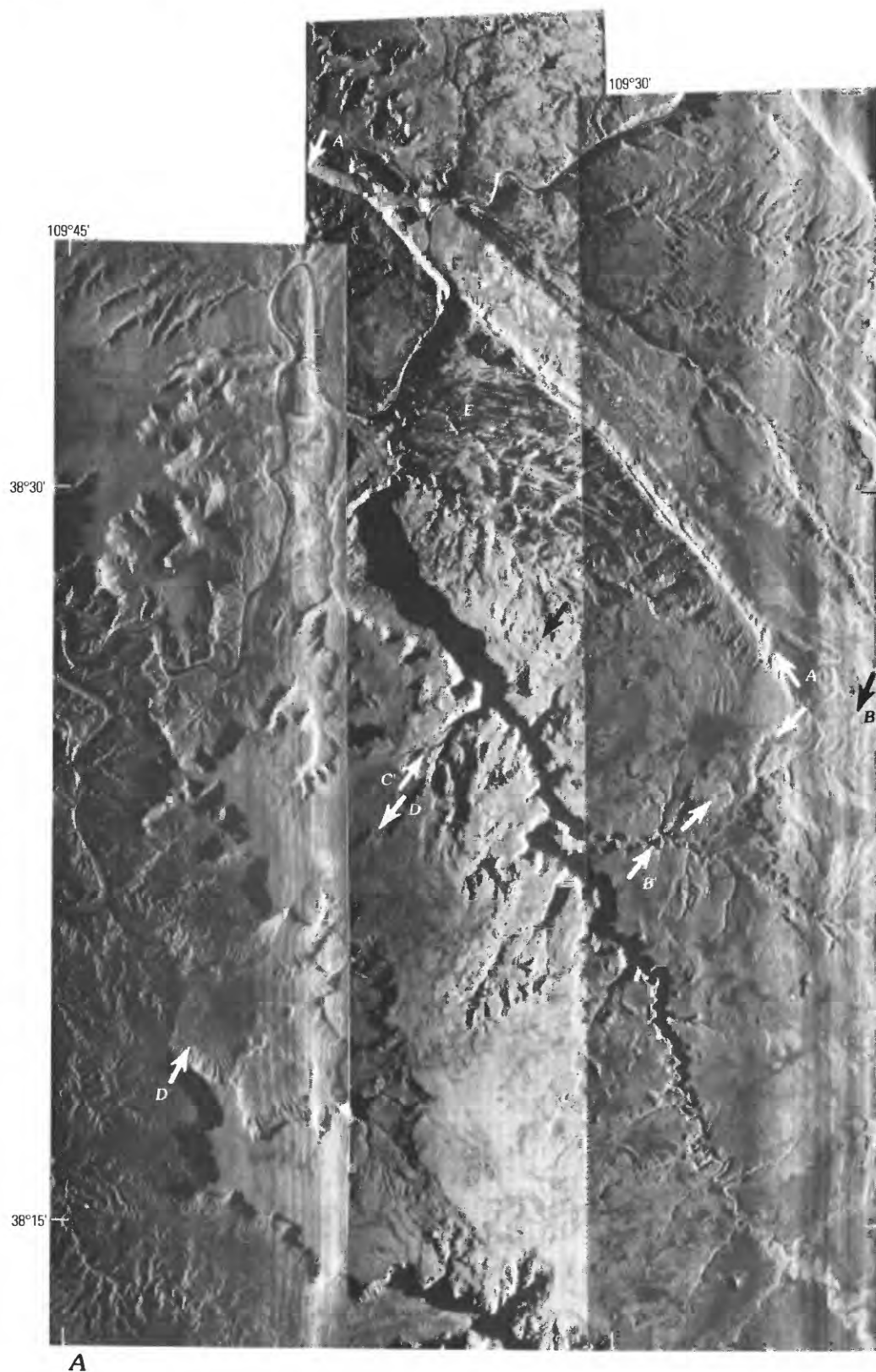


The Moab quadrangle coverage as planned is shown in figure 3. Approximately the western three-fifths of the quadrangle is covered. In actuality, all of the passes include some sidelap, except for an omitted strip 0.8 mi (1.3 km) wide between lines 5 and 6. Areas that are contained in the sidelap coverage were imaged at the two angles. For example, if an area of interest was imaged at the distal edge of one swath, its depression angle would have been approximately 13°. On the next pass, the same scene would have been imaged at a depression angle of 57° if there was no side lap. This large change in depression angle allows reflectivity studies to be made over a 44° angular difference from a single data set. The geometry of the sidelap is shown in figure 4 (R.F.

Rawson, Canada Center for Remote Sensing, written commun., 1980).

### SLANT-RANGE SCALE DISTORTION

A slant-range image presentation involves a constant cathode-ray tube (CRT) sweep rate across each line. Consequently, the spacing between return signals on slant-range imagery is directly proportional to the time interval between echoes from adjacent terrain features. This interval is directly proportional to the slant, rather than the horizontal, distance between the sensor and any given





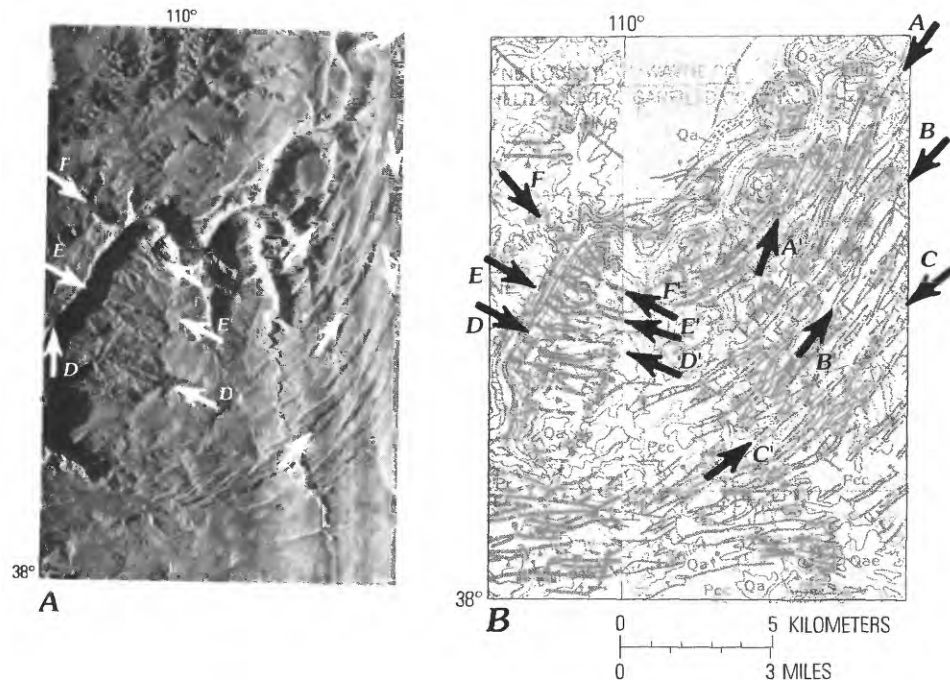


**Figure 8.** Needles fault zone, Canyonlands, Utah (Moab and Salina  $1^{\circ}\times 2^{\circ}$  quadrangles). Curved northeast-trending Needles fault zone consists predominantly of high-angle horst and graben structures; for example,  $A-A'$ ,  $B-B'$ ,  $C-C'$ , and many others. West-northwest-trending faults or fractures heretofore mapped only on the east bank of the Colorado River in this area are visible on the radar image, such as at  $E-E'$ . *A*, X-band radar image. *B*, Geologic structure. Modified from Williams (1964) and Williams and Hackman (1971).

object. In a ground-range image presentation, the CRT sweep incorporates a hyperbolic timing correction in which the spacing between image points is approximately proportional to the horizontal ground distance between terrain features.

Figure 1 illustrates the characteristics of slant-range and ground-range images. *A*, *B*, and *C* represent objects of equal size that are equally separated in the near, middle, and far range. The respective ground ranges to the points are  $GR_A$ ,  $GR_B$ , and  $GR_C$ . Based directly on the signal return time, the slant-range image shows unequal distances between the features, as well as unequal widths for the features. The result is a variable image scale that is at a minimum in the near range and progresses hyperbolically to a maximum at the far range, as described in the previous section. Therefore, on a slant-range presentation, object width  $A_1 < C_1$  and distance  $AB < BC$ . Applying a hyperbolic correction, a ground-range image of essentially constant scale can be constructed with width  $A=B=C$  and distance  $AB=BC$ .

Obviously, the scale distortions inherent in slant-range images preclude their direct use for accurate planimetric mapping. However, approximate ground range ( $GR$ ) can be derived from slant range ( $SR$ ) and flying height ( $H$ ) under the assumption of flat terrain. From figure 1

$$SR^2 = H^2 + GR^2,$$

so

$$GR = (SR^2 - H^2)^{1/2}.$$

Therefore, a ground-range distance can be calculated from a slant-range distance if the flying height is known. The assumption of flat terrain, not a characteristic of the Moab  $1^{\circ}\times 2^{\circ}$  quadrangle, should be noted, however. Flight parameters also affect both range and azimuth scales. The range scale changes with changes in aircraft altitude, and the azimuth scale is a function of precise synchronization between the aircraft ground speed and the proportional film transport speed past the CRT (adapted from Lillesand and Kiefer, 1987).

## TECTONIC INTERPRETATION OF SELECTED RADAR IMAGES

Five selected areas within the northern Paradox Basin are shown in figures 5–9, which compare the X-band radar images with similar parts of geologic structure maps (Williams, 1964; Williams and Hackman, 1971).

The uncontrolled radar images show more topographic and structural detail than smaller scale rectified Landsat

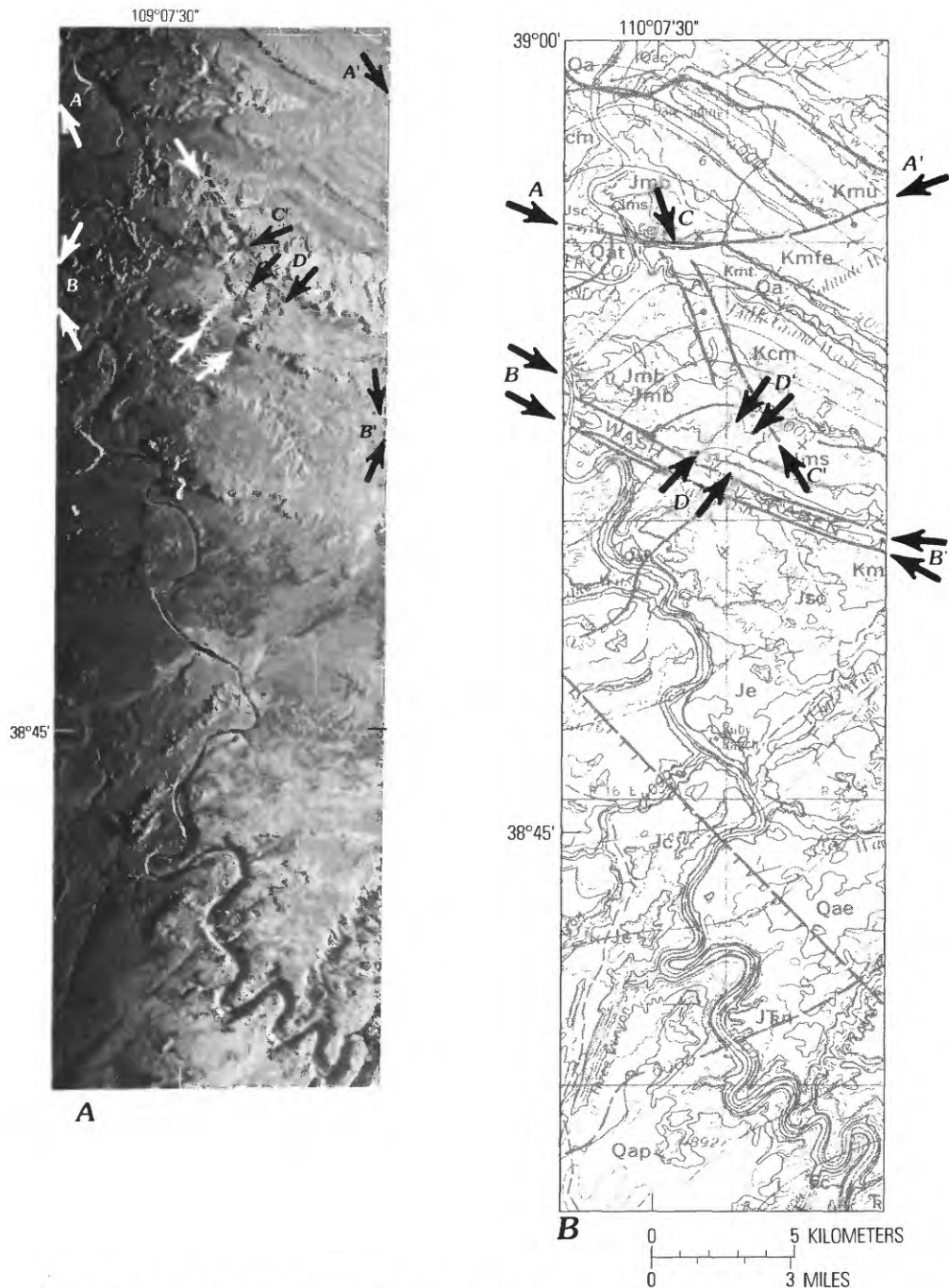


**Figure 9.** Green River area between Salt Wash and Cottonwood grabens, Salina  $1^{\circ} \times 2^{\circ}$  quadrangle, Utah. *A-A'*, Cottonwood graben fault. Note drag effect and right lateral offset of Cretaceous beds. South flank of fault zone is also downdropped, indicating complex, perhaps scissors or recurrent, movement along this fault. *B-B'*, Salt Wash graben, perhaps relatively superficial. *C-C'*, north-northwest-trending high-angle faults cutting Cretaceous and Jurassic beds at *C*. *D-D'*, previously unmapped fractures or faults trending  $N. 40^{\circ} E$ . *A*, X-band radar image. *B*, Geologic structure. Modified from Williams and Hackman (1971).

multispectral scanner images (Friedman and Simpson, 1978, 1980; Friedman and others, 1979, this volume), but azimuthal bearings of linear features of the radar images are not as accurate as those depicted on the Landsat multispectral

scanner images. By comparing the radar images with the Landsat multispectral scanner images and with geologic structure maps, the approximate strike of linear features observed on the radar images can be reliably inferred.

The radar images display a strong N. 37°–65° E. trend representing joint sets (for example, *G* of fig. 6) (Friedman and Simpson, 1978, p. 26–28) and extensional vertical fracture systems having little or no offset (for example, *F–F'* and *G–G'* of fig. 5 and *D–D'* of fig. 9). The N. 37°–65° E. trend is also represented by extensional high-angle faults of Laramide and post-Laramide age that show predominantly vertical offset (Weir and others, 1961; Hinrichs and others, 1968), as exemplified by *B–B'* and *C–C'* (of figure 7), which cut the Spanish Valley and Cane Creek anticlines, respectively. A fault set of similar northeasterly strike cutting Lockhart Basin northeast of Gibson Dome is discernible between *D* and *D'*, also in figure 7. The complexity of the curved, generally northeast trending horst and graben terrane of the Needles fault zone of Canyonlands is clearly shown in figure 8.

A clear example of stratigraphic offset and structural drag along the right-lateral or scissors Cottonwood graben fault is shown at *A–A'* in figure 9, near the Green River in the Salina 1°×2° quadrangle.

The dominant (or first-order) strike frequency of major lineaments (more than 20 km long (12.4 mi) and faults in this part of the Paradox Basin is N. 40°–60° W. and is best exemplified on the radar images by *A–A'*, the Moab fault system of figure 7. The Moab fault trend coincides with the dominant gravity- and magnetic-field trends and is generally parallel to the fold axes of the major salt anticlines of the northern Paradox Basin and, in a less direct sense, to the southwestern boundary fault zone of the Uncompahgre uplift (Elston and Shoemaker, 1961; Williams, 1964; Friedman and Simpson, 1978).

The location and strike of both northwest and northeast lineament sets may reflect deep-seated control by tectonic trends and discontinuities of the Precambrian surface as delineated in the gravity and magnetic fields (Case and Joesting, 1972, pls. 1–3). Structures *A–A'*, *B–B'*, *C–C'*, and *D–D'* of figure 7 may represent the surface reflection of the forementioned geophysical trends of the Precambrian surface.

Based on field observations of M.N. Grout (written commun., 1991), joint sets, examples of which are clearly imaged by X-band radar and shown in this report, are of Laramide and post-Laramide age. Rose diagrams of 294 joint measurements by the senior author in the region between Deadhorse Point and Salt Valley, and mostly in

Jurassic stratigraphic units, demonstrate an azimuthal range of N. 52° W.–N. 65° E. in at least four sets. The joint sets to the northwest are oldest and those to the northeast are youngest, perhaps implying a clockwise tectonic rotation of the Paradox Basin and surrounding part of the craton in relation to the continental interior.

## REFERENCES CITED

- Case, J.E., and Joesting, H.R., 1972, Regional geophysical investigations in the central Colorado Plateau: U.S. Geological Survey Professional Paper 736, 31 p.
- Doelling, H.H., 1985, Geology of Arches National Park: Utah Geological and Mineral Survey Map 74.
- Elston, D.P., and Shoemaker, E.M., 1961, Preliminary structure contour map on top of salt in the Paradox Member of the Hermosa Formation in the salt anticline region, Colorado and Utah: U.S. Geological Survey Oil and Gas Investigations Map OM-209.
- Friedman, J.D., Case, J.E., Simpson, S.L., 1979, Tectonic implications of lineaments of the northern Paradox basin, Utah-Colo- rado [abs.]: EOS, v. 60, no. 17, p. 396–397.
- Friedman, J.D., and Simpson, S.L., 1978, Landsat investigations of the northern Paradox basin, Utah and Colorado—Implications for radioactive waste emplacement; Part 1, Lineaments and alignments: U.S. Geological Survey Open-File Report 78–900, 49 p.
- 1980, Lineaments and geologic structure of the northern Paradox basin, Colorado and Utah: U.S. Geological Survey Miscellaneous Field Studies Map MF-1221.
- Hinrichs, E.N., Krummel, W.J., Jr., Moore, H.J., 3rd, and Connor, J.J., 1968, Geologic map of northeast quarter of the Hatch Point quadrangle, San Juan County, Utah: U.S. Geological Survey Miscellaneous Geologic Investigations Map I-526.
- Lillesand, T.M., and Kiefer, R.W., 1987, Remote sensing and image interpretation (2nd ed.): New York, John Wiley and Sons, 721 p.
- Weir, G.W., Kennedy, V.C., Puffett, W.P., and Dodson, C.L., 1961, Preliminary geologic map and section of the Mount Peale 2° NW quadrangle, San Juan County, Utah: U.S. Geological Survey Miscellaneous Field Studies Map MF-152, scale 1:24,000.
- Williams, P.L., 1964, Geology, structure, and uranium deposits of the Moab quadrangle, Colorado and Utah: U.S. Geological Survey Miscellaneous Geological Investigations Map I-360, scale 1:250,000.
- Williams, P.L., and Hackman, R.J., 1971, Geology, structure, and uranium deposits of the Salina quadrangle, Utah: U.S. Geological Survey Miscellaneous Geological Investigations Map I-591, scale 1:250,000.